Myhre, A.M., Thiede, J., Firth, J.V., et al., 1995
Proceedings of the Ocean Drilling Program, Initial Reports, Vol. 151

10. SITE 912[1]

Shipboard Scientific Party[2]

HOLE 912A

Date occupied: 27 August 1993

Date departed: 28 August 1993

Time on hole: 20 hr, 45 min

Position: 79°57.557′N, 5°27.360′E

Bottom felt (drill pipe measurement from rig floor, m): 1047.9

Distance between rig floor and sea level (m): 11.14

Water depth (drill pipe measurement from sea level, m): 1036.8

Total depth (from rig floor, m): 1193.3

Penetration (m): 145.4

Number of cores (including cores with no recovery): 16

Total length of cored section (m): 145.4

Total core recovered (m): 118.37

Core recovery (%): 81.4

Oldest sediment cored:
Depth (mbsf): 145.4
Nature: silty clay
Earliest age: Pliocene

HOLE 912B

Date occupied: 28 August 1993

Date departed: 28 August 1993

Time on hole: 10 hr, 45 min

Position: 79°57.533′N, 5°27.397′E

Bottom felt (drill pipe measurement from rig floor, m): 1048.6

Distance between rig floor and sea level (m): 11.14

Water depth (drill pipe measurement from sea level, m): 1037.5

Total depth (from rig floor, m): 1089.1

Penetration (m): 40.5

Number of cores (including cores with no recovery): 5

Total length of cored section (m): 40.5

Total core recovered (m): 41.77

Core recovery (%): 103.1

Oldest sediment cored:
Depth (mbsf): 40.5
Nature: silty clay
Earliest age: Quaternary

[1]Myhre, A.M., Thiede, J., Firth, J.V., et al., 1995. *Proc. ODP, Init. Repts.*, 151: College Station, TX (Ocean Drilling Program).

[2]Shipboard Scientific Party is as given in the list of participants preceding the Table of Contents.

HOLE 912C

Date occupied: 12 September 1993

Date departed: 13 September 1993

Time on hole: 1 day, 30 min

Position: 79°57.523′N, 5°27.363′E

Bottom felt (drill pipe measurement from rig floor, m): 1048.0

Distance between rig floor and sea level (m): 11.38

Water depth (drill pipe measurement from sea level, m): 1036.6

Total depth (from rig floor, m): 1257.1

Penetration (m): 209.1

Number of cores (including cores with no recovery): 12

Total length of cored section (m): 115.6

Total core recovered (m): 5.91

Core recovery (%): 5.1

Oldest sediment cored:
Depth (mbsf): 209.1
Nature: silty clay
Earliest age: Pliocene

Principal results: Site 912 is located on the shallow southwestern edge of the Yermak Plateau. The site was selected to study trends in Neogene and Quaternary sediment accumulation on the Yermak Plateau and to investigate the glacial history of the Arctic gateway. Site 912 had been planned for penetration through a thick sedimentary section of Quaternary and Neogene age with evidence for the glacial history of the Arctic Ocean, the history of the North Atlantic (West Spitsbergen Current) water influx into the Arctic Ocean. It also was to be an intermediate member of a depth transect.

When we arrived at the planned location, which was easily verified by seismic reflection profiling during the approach, sea ice was detected at a sufficient distance to begin drilling operations. However, during APC-coring of the first hole, the ice edge advanced rapidly, forcing us to abandon drilling operations and pull back to close to the seafloor. After the ice edge had settled down, we renewed our efforts by starting a second APC hole, which to our dismay also had to be abandoned after a few cores, this time permanently because of the eastward advancing ice.

Hole 912A reached 145.4 mbsf, and Hole 912B only 40.5 mbsf. Toward the end of Leg 151, we returned to Site 912 and drilled Hole 912C. The aim was to RCB-core the deeper part of the section; however, this hole (with very low recoveries) also had to be abandoned after it reached 209.1 mbsf, because of advancing ice. The stratigraphic record of this site, therefore, is too short to reach all scientific objectives.

Sediments recovered at Site 912 are predominantly very dark gray, unlithified, slightly to moderately bioturbated silty clays and clayey silts of Pliocene to Quaternary age. Faint color banding, possibly of diagenetic origin, is present in intervals throughout. Sediment texture and mineral abundances exhibit variations of approximately 20%–30% throughout the sequence, but no major trends occur. A single lithologic unit was defined at Site 912 based on the relative uniformity in sediment type, texture, and mineralogy. The unit is characterized by higher abundances and greater

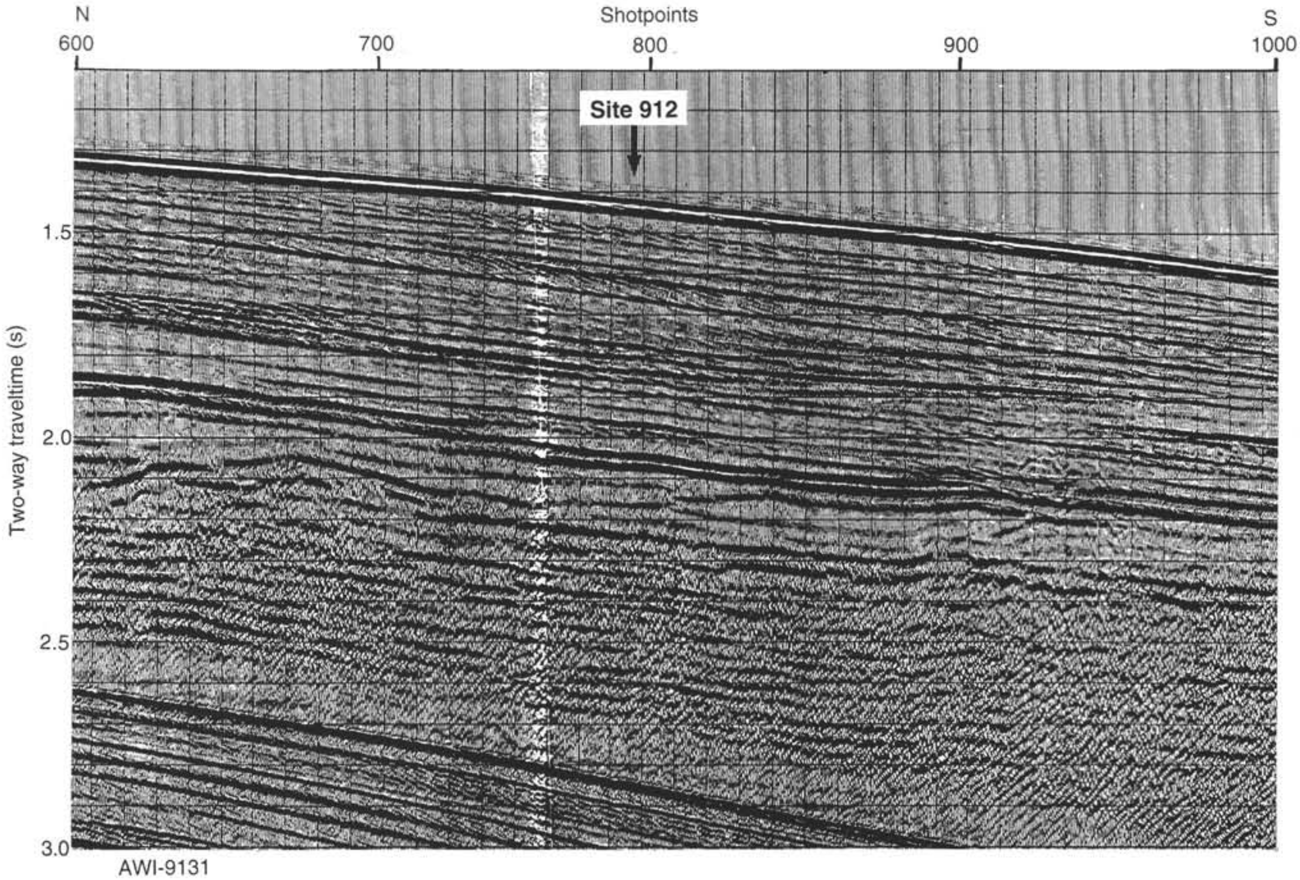

Figure 1. Multichannel seismic line AWI-9131, showing location of Site 912 at shotpoint 790.

sizes of dropstones as compared with Sites 910 and 911 on the inner Yermak Plateau. Most of the dropstones consist of silt-, sand-, and mudstones, but metamorphic and igneous rocks are also common. Two lithologic subunits were defined on the basis of changes in dropstone abundance, with the Subunit IA/IB boundary placed at 40 mbsf (within the Quaternary). The uphole increase in dropstone abundance at about 40 mbsf indicates an enhancement of glacio-derived sediment transport potentially related to an intensification of Northern Hemisphere glaciation. Minor differences in dropstone lithologies between the subunits could indicate slight changes in ice circulation and source areas.

Three holes recovered a Quaternary and Pliocene sequence of ice-rafted sediments with scattered occurrences of calcareous microfossils. Siliceous microfossils are absent, with the exception of rare reworked diatoms and silicoflagellates, rare and poorly preserved radiolarians, and rare diatoms indicative of uppermost Pliocene to lower upper Quaternary. Dinoflagellates are rare and non-age-diagnostic; terrestrial palynomorphs are common throughout. Ice-rafted *Inoceramus* prisms are found in Pliocene sediments.

The magnetostratigraphic results yield a fairly robust age vs. depth model, which is consistent with biostratigraphic age determinations. Because of poor core recovery, estimation of Pliocene linear sedimentation rates was not possible. Pre-Jaramillo sedimentation rates vary from 80 to 100 m/m.y., but they decrease to about 30 m/m.y. during the last 1 m.y. of deposition.

The physical properties allowed subdivision of the sequence into three geotechnical units. The upper one (geotechnical Unit I, to 8 mbsf) comprises highly variable, but generally low bulk density and high porosity silty clay without dropstones. Geotechnical Unit II (8–50 mbsf) consists of silty clay to mud with variable amounts of dropstones and increased, but highly variable, bulk densities, as well as inversely related trends in water content and porosity. In Geotechnical Unit III (below 50 mbsf), recovery is reduced, but physical properties appear more constant. The recovered sediments suggest a hemipelagic, glacio-marine depositional environment, the dominant proportion of the material being relatively fine-grained.

BACKGROUND AND OBJECTIVES

Site 912 (proposed site YERM 2A) (see Fig. 17 of "Introduction" chapter, this volume) is located on the southwestern slope of the Yermak Plateau in water depths of about 1050 m, on the upper part of the slope that dips into the Molloy Rift and Spitsbergen Fracture Zone (see Figs. 6 and 7 of "Introduction" chapter, this volume). Site 912 is about 45 km Southwest of Site 910, which is the most shallow site on the Yermak Plateau. Site 912 is located on multichannel seismic line AWI-9131, shotpoint 790, which has been recorded running almost North-South parallel to the major features of the margin, (Fig. 1). A strong seafloor multiple is masking the deeper part of the section, but a sequence of sediments probably more than 1300 m thick can be recognized, although basement is not observed. Sequences of continuous, strong amplitude, high-frequency, and gently southwestward dipping reflectors can be observed in the upper part of the seismic section. These are alternating with sequences characterized by continuous reflectors of very low amplitude that sometimes contain short high-amplitude segments. In the deeper part of the section the reflectors have a more low-frequency character with varying amplitude, and the reflectors are difficult to trace over longer distances. Several

Table 1. Coring summary, Holes 912A, 912B, and 912C.

Core	Date (1993)	Time (UTC)	Depth (mbsf)	Length cored (m)	Length recovered (m)	Recovery (%)
151-912A-						
1H	Aug. 27	1750	0.0–4.0	4.0	4.00	100.0
2H	Aug. 27	1805	4.0–13.5	9.5	9.93	104.5
3H	Aug. 27	1825	13.5–23.0	9.5	9.90	104.2
4H	Aug. 27	1915	23.0–32.5	9.5	10.06	105.9
5H	Aug. 27	1940	32.5–42.0	9.5	10.05	105.8
6H	Aug. 27	2010	42.0–51.5	9.5	10.23	107.7
7H	Aug. 27	2055	51.5–61.0	9.5	10.33	108.7
8H	Aug. 27	2120	61.0–70.5	9.5	10.28	108.2
9X	Aug. 27	2250	70.5–78.0	7.5	8.72	116.3
10X	Aug. 27	2335	78.0–87.6	9.6	8.01	83.4
11X	Aug. 28	0035	87.6–97.2	9.6	9.62	100.2
12X	Aug. 28	0215	97.2–106.9	9.7	0.00	0.0
13X	Aug. 28	0245	106.9–116.5	9.6	8.44	87.9
14X	Aug. 28	0325	116.5–126.1	9.6	0.00	0.0
15X	Aug. 28	0415	126.1–135.8	9.7	8.65	89.2
16X	Aug. 28	0510	135.8–145.4	9.6	0.15	1.6
Coring totals				145.4	118.37	81.4
151-912B-						
1H	Aug. 28	1035	0.0–5.3	5.3	5.31	100.2
2H	Aug. 28	1055	5.3–14.8	9.5	9.88	104.0
3H	Aug. 28	1115	14.8–24.3	9.5	9.94	104.6
4H	Aug. 28	1145	24.3–31.0	6.7	6.66	99.4
5H	Aug. 28	1255	31.0–40.5	9.5	9.98	105.1
Coring totals				39.5	41.77	103.1
151-912C-						
1R	Sept. 12	1150	93.5–103.1	9.6	0.15	1.6
2R	Sept. 12	1240	103.1–112.7	9.6	0.08	0.8
3R	Sept. 12	1345	112.7–122.4	9.7	0.08	0.8
4R	Sept. 12	1420	122.4–132.0	9.6	0.03	0.3
5R	Sept. 12	1520	132.0–141.7	9.7	0.30	3.1
6R	Sept. 12	1615	141.7–151.3	9.6	0.03	0.3
7R	Sept. 12	1650	151.3–160.9	9.6	0.28	2.9
8R	Sept. 12	1725	160.9–170.6	9.7	0.76	7.8
9R	Sept. 12	1820	170.6–180.2	9.6	0.08	0.8
10R	Sept. 12	1905	180.2–189.9	9.7	0.00	0.0
11R	Sept. 12	2020	189.9–199.5	9.6	0.72	7.5
12R	Sept. 12	2115	199.5–209.1	9.6	3.40	35.4
Coring totals				115.6	5.91	5.1

sedimentary wedges and unconformities can be mapped, some indicating erosional features. As the multichannel seismic line is oblique to the general dip direction, it is difficult to find any obvious pattern to the variation in the thicknesses of the sequences. This site is located in an area swept by the West Spitsbergen Current, resulting in a high temporal variability of sedimentation (Manley et al., 1992).

Based on deep multichannel seismic data, Eiken (1993) suggests that the continent/ocean boundary is located under the upper slope in this region, and Site 912 might be situated on oceanic crust. We refer to the "Site 910" chapter (this volume) for general geological background information of this region.

Scientific Objectives

Site 912 was planned as an intermediate member of a bathymetric transect across the Yermak Plateau. The purpose of the site was to study the Neogene and Quaternary glacial history of the Arctic Ocean and the history of North Atlantic Ocean surface water influx to the Arctic. The site was also suggested as an alternate site for YERM-1 if that was not accessible. Site 912, however, was not to be drilled to basement, and its water depth is 150 m deeper than YERM-1.

OPERATIONS

Transit to Site 912

The 35-nmi transit to Site 912 required 3.6 hr for an average speed of 9.7 kt. The seismic survey started at 1136 hr, 27 August, and covered 13 nmi in 2.3 hr at 5.6 kt. A Datasonics 354B beacon was dropped at 1256 hr, the seismic gear retrieved, and the ship returned to location.

Hole 912A

The *Fennica* found some scattered ice on location and pushed it away before the *Resolution* arrived. The closest ice to the location was a 15-nmi-long by 0.1-nmi-wide ice tongue about 5.2 nmi from the location at heading 335°.

An advanced hydraulic piston corer/extended core barrel (APC/XCB) bottom-hole assembly (BHA) was run. The precision depth recorder (PDR) indicated a water depth of 1048.4 mbrf. Core 151-912A-1H established the water depth as 1047.9 mbrf. Cores 151-912A-1H through -8H were taken from 0.0 to 70.5 mbsf, with 70.5 m cored and 74.8 m recovered (106.2% recovery) (Table 1). APC-coring was terminated after Core 8H because it was a very hard claystone. Cores were not oriented because of the high latitude. The Adara temperature shoe was run on Cores 4H and 7H. The formation was extremely stiff, compacted, gray, silty clay with occasional ice-rafted debris (IRD) pebbles and a hard claystone at the bottom.

The XCB-coring assembly was run, and Cores 151-912A-9X through -16X were taken from 70.5 to 145.4 mbsf, with 74.9 m cored and 43.59 m recovered (58.2% recovery). The shoe of Core 151-912A-16X contained about 0.15 m of dolostone (probably a large ice-rafted dropstone).

The ice tongue had been moving South-Southwest at about 0.5 kt with the current from the North and wind from the East. The *Fennica* attempted to push and wash the ice away from the *Resolution* with some success, but the ice tongue was too large and closing back together. The *Fennica* reported it could not move one ice block 20 m × 30 m × 15 m. It appeared the ice would pass along a line 0.5 nmi South-Southwest of the ship, and at 0515, 28 August, the ice tongue approached within 1.5 nmi of the ship moving at 0.3 kt. The bit was pulled to within one stand of the seafloor as a precaution. The ice moved South-Southeast of the ship, stopped, reversed course, and seemed to stall about 1 nmi North of the ship.

Hole 912B

Hole 912B was spudded in the interim after 1 hr observing the ice. The ice seemed to be slowing down to 0.2 kt, which would allow enough time to core a second shallow APC hole for high-resolution studies. Core 151-912B-1H established the water depth as 1048.6 mbrf. Cores 151-912B-1H through -5H were taken from 0.0 to 40.5 mbsf, with 40.5 m cored and 41.77 m recovered (103.1% recovery). No cores were oriented because of the high latitude, and no temperatures were measured. The formation was extremely stiff, compacted, gray, silty clay with occasional IRD pebbles.

The ice had continued to move toward the ship at 0.2 kt despite attempts by the *Fennica* to push and wash it back. APC-coring was terminated after Core 151-912B-5H because the ice moved to within 0.3 nmi of the *Resolution*, and the *Fennica* was unable to open a path for the ship or control the many 6 m × 2 m × 2 m blocks advancing on a 3-nmi front. One block of ice 20 m × 30 m × 15 m could not be controlled at all. Additional large ice floes were seen on radar in the area.

The pipe was pulled above the seafloor at 1350 hr. The *Resolution* moved one mile away in dynamic positioning (DP) mode to monitor the ice, which stayed on the location until 1800 hr, when a decision was made to return to Site 910. The bit was pulled through the rotary table at 2017 hr, 28 August, ending Hole 912B. Two beacons were left on location because they were covered by the ice field.

Return to Site 912

After Site 909 was completed, another attempt was made to core on the Yermak Plateau. At the time, only Site 912 was open. The 87-nmi transit from Site 909 to Site 912 required 7.75 hr for an average speed of 11.2 kt. The site had been surveyed previously, so no seismic survey was conducted. The original Datasonics beacons were still operating, but a single Benthos 210 beacon was dropped (in case the ice returned and forced the ship off location again) at the original global positioning system (GPS) position (South and East of the Holes 912A and 912B). The two Datasonic beacons that were originally left on site were recalled and recovered. The *Fennica* reported that the edge of the pack ice was to the Northwest, 4.9 nmi away and moving Southeast at 0.3 kt. The ice consisted of heavy ice up to 4 m thick, with 100% cover and ridges 2 m high.

Hole 912C

An RCB BHA was run. The water depth was 1048.0 mbrf, and Hole 912C was spudded at 0700 hr, 12 September. The hole was drilled from 0.0 to 93.5 mbsf. Cores 151-912C-1R through -12R were taken from 93.5 to 209.1 mbsf, with 115.6 m cored and 5.91 m recovered (5.1% recovery). Heat flow measurements performed in Hole 912A indicated a temperature gradient of 64.8°C/km.

The ice edge continued to advance to the East-Southeast, and at 2115 hr forced us to pull up to 60 mbsf with the ice only 1.69 nmi away, moving toward us at 0.6 kt. At 2215 hr, the ice edge had advanced to within 1.25 nmi, and the bit was pulled above the seafloor. The ice edge continued to advance, and it was obvious that the location could not be drilled; therefore, the bit was pulled up to the ship, clearing the rotary table at 0120 hr, 13 September.

Fennica Leaves

An ice breaker would probably not be required at the next site (EGM-2), so the *Fennica* was called back to the *Resolution* for a final fuel gauge check, and released at 0140 hr, 13 September.

LITHOSTRATIGRAPHY

Introduction

The lithostratigraphic summary is largely based on Hole 912A (0–145.4 mbsf) because Hole 912B only reached 40.5 mbsf and Hole 912C (93.5–209.1 mbsf) had a recovery of only 5.1%. Data from below 140 mbsf are not presented in the lithologic summary chart (Fig. 2) because of the low recovery in this depth interval.

Sediments recovered at Site 912 (Holes 912A, 912B, and 912C) are predominantly very dark gray, unlithified, structureless to moderately bioturbated silty clays and clayey silts of Pliocene to Quaternary age. Faint color banding, probably of diagenetic origin, is present in intervals throughout. Sediment texture and particle abundances (Fig. 2) exhibit variations of ~20%–30% throughout the sequence, but no major trends occur.

Silty mud and clayey mud, mainly interbedded with finer-grained sediment, occur as minor lithologies throughout the sequence (Fig. 2). The mud layers are characterized by a more brownish very dark gray color and a slightly coarser texture on the split core surface. Layers of dark gray clay occur only in the upper 15 m of the sequence. Inorganic carbonate grains form distinct layers, with up to 40% carbonate, and occur as a background concentration of ~5% throughout the sequence (Fig. 2). Carbonate grains are typically silt-sized and similar to carbonates described in the site chapters for Sites 908–911. Nevertheless, in some mud layers the carbonate grains are more irregular in shape, and sand-sized grains occur.

A single lithostratigraphic unit was defined at Site 912 based on the relative uniformity in sediment type, texture, and mineralogy. The unit is characterized by higher abundance of dropstones and greater sizes of dropstones compared with Sites 910 and 911 on the inner Yermak Plateau. The amount of dropstones varies between 0 and 28 per core, with the highest abundances above 40 mbsf (Fig. 3). The size distribution is fairly constant throughout the sequence, and no major trends are recorded (Fig. 4 and Table 2). Dropstones occur in all lithologies, although they are most common in mud layers. Most of the dropstones consist of siltstones, sandstones, and mudstones, but metamorphic and igneous rocks are also common. The abundance of biogenic material in the recovered sediments is very low, and most intervals are barren of microfossils according to smear slide analyses. Biocarbonate is found from 0 to 38 mbsf, and biosilica is present in trace amounts in the interval 80–209.1 mbsf. No ash layers are present in the sediments from this site.

Two lithologic subunits were defined on the basis of changes in dropstone (≥1 cm) abundance (Table 3). The subunit boundary is placed at 40 mbsf, where the dropstone abundance decreases downhole from about 15 to <10 per core. The location of the boundary is supported by a change in the trace biogenic component from calcareous to siliceous microfossils. The downhole extent of Subunit IB is uncertain because of the low recovery between 145 and 209.1 mbsf. However, on the basis of the recovered sediments, the entire sequence below 40 mbsf is believed to be the same subunit.

The entire stratigraphic unit is interpreted to have been deposited in a hemipelagic environment with a large input of ice-rafted terrigenous materials during cold high-latitude climate conditions.

Lithologic Subunit IA:

Sections 151-912A-1H-1 through -5H-5, 150 cm (0–40.0 mbsf), 151-912B-1H-1 through -5H-CC (0–40.5 mbsf)
Thickness: 40.0 m
Age: Quaternary

Throughout the subunit, up to 1.5-m-thick layers of very dark gray and olive gray silty clay alternate. The color changes do not correlate with changes in composition of the coarse fraction or the biogenic content of the sediment, and may be of diagenetic origin. Silty

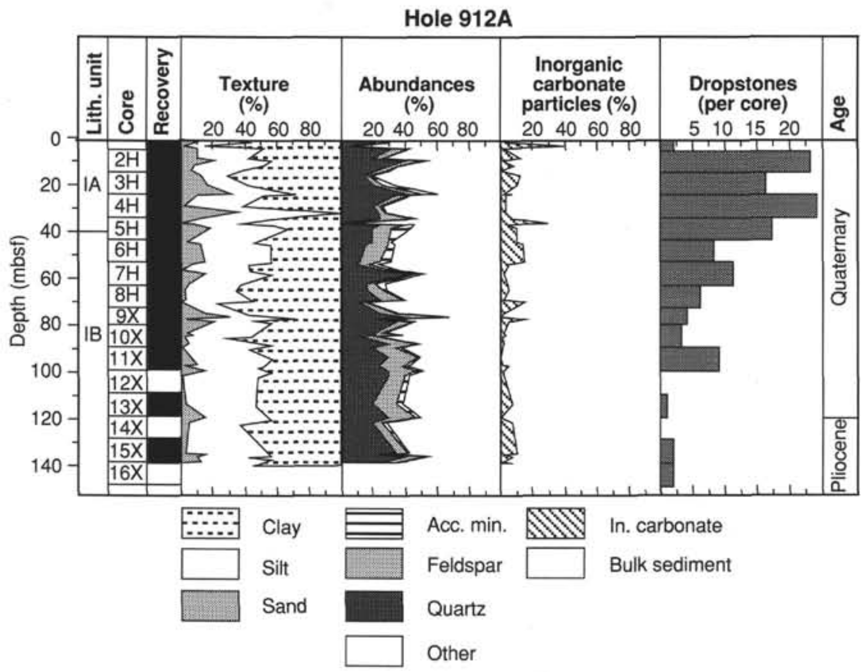

Figure 2. Texture, particle abundance, inorganic carbonate particle content, and dropstone abundance (per core) vs. depth for Hole 912A. Recovery, lithostratigraphic units, and age based on paleontology are shown.

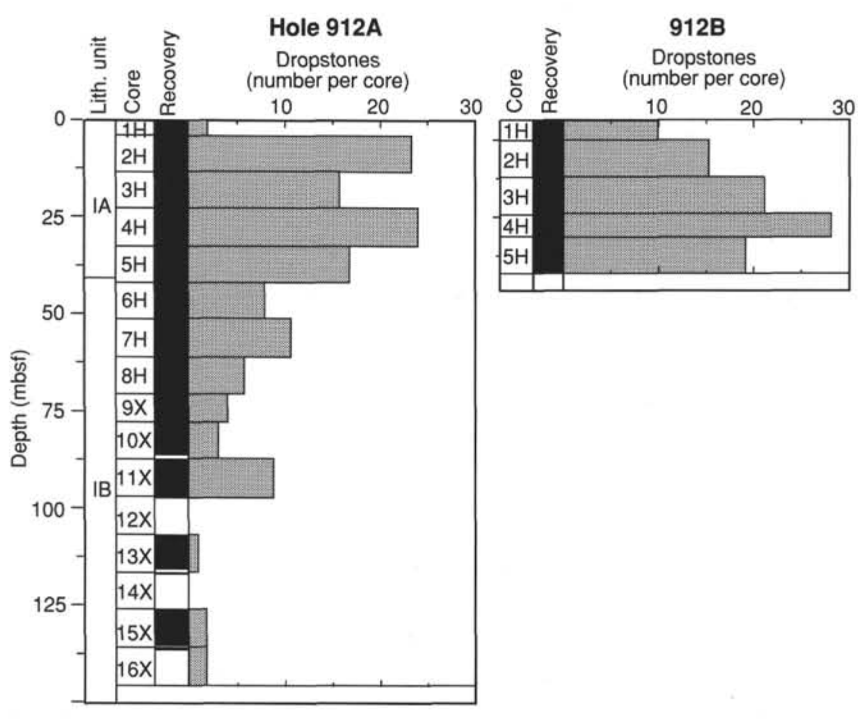

Figure 3. Abundance of dropstones (≥1 cm) in Holes 912A and 912B. The values are not normalized to 100% recovery. Note the downhole decrease in dropstone abundance at 40 mbsf, which marks the boundary between the lithostratigraphic subunits.

mud and clayey mud, predominantly very dark gray, are interbedded with silty clay throughout the subunit (Fig. 5). As a result of bioturbation, most contacts are gradational, but some mud layers have sharp bases (Fig. 5). In general, the silt and sand component of the mud layers are similar to the major lithology in particle abundance. Dark gray clay occurs in some intervals, commonly as part of a normally graded fining-upward sequence from clayey mud through silty clay. Fining-upward sequences are most common above 12 mbsf, typically with thicknesses of about 20 cm. Clay- and silt-sized carbonate grains are present in all lithologies, varying in abundance from 2% to 40% (Fig. 2). The highest abundances of inorganic carbonate particles are found in mud layers, including up to 5% sand-

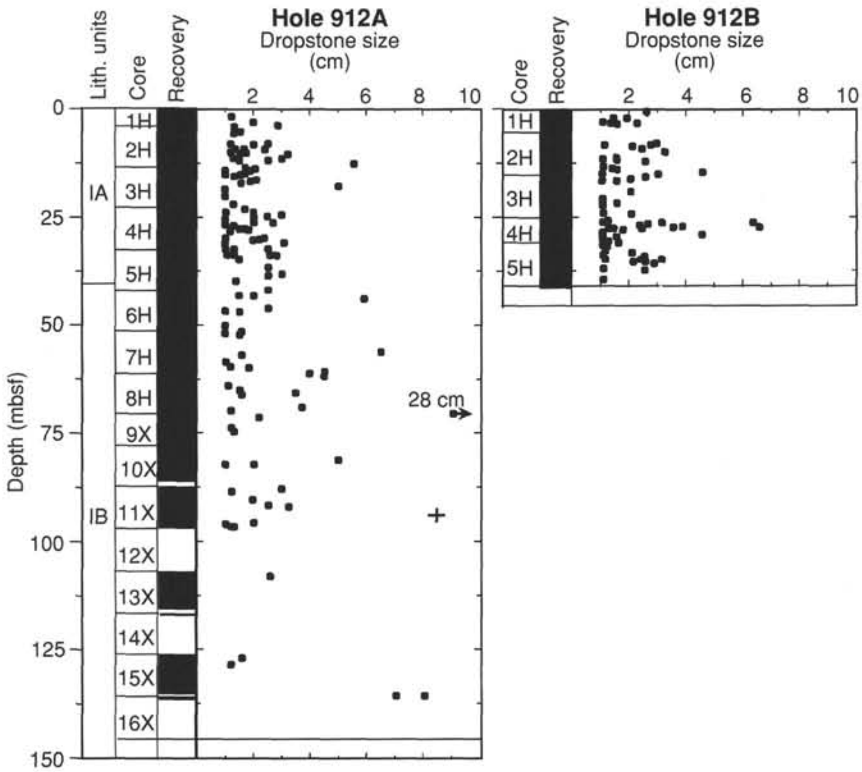

Figure 4. Size of dropstones (≥1 cm) in Holes 912A and 912B. The single dropstone found in Hole 912C is marked by a cross. Note the range of dropstone sizes between 1 and 8 cm and the large dropstone at 70.6 mbsf, with a length of one axis of 28 cm.

sized grains. In all lithologies the coarse fraction is dominated by quartz (Fig. 2). Feldspar, mica, opaques, and accessory minerals occur in minor amounts.

The number of dropstones (diameter ≥1 cm) per core varies between 10 and 28 with an average of about 15 (Fig. 3). No obvious correlation is observed between dropstone abundances in Hole 912A and those in Hole 912B, although the highest concentration seems to be near 30 mbsf and the lowest at the top of Subunit IA. The size of the dropstones (≥1 cm) is variable, with a diameter up to 7 cm (Fig. 4). However, most dropstones have sizes between 1 and 3 cm. The dropstones are mainly sedimentary in origin, but igneous and metamorphic rocks are also fairly common in this subunit (Table 2). Smear-slide data typically reveal trace abundances of foraminifers and nannofossils, but 2%–6% is found in four distinct layers of carbonate mud (0.65–1.3 mbsf, 12.6–12.8 mbsf, 19.56–20.0 mbsf, and 37.0–37.4 mbsf).

Lithologic Subunit IB:

Sections 151-912A-5H-6, 0 cm, through -16H-1 (40.0–145.4 mbsf), 151-912C-1R-1 through -12R-CC (93.5–209.1 mbsf)
Thickness: 169.1 m
Age: Pliocene to Quaternary

Subunit IB consists of silty clay and clayey silt, in most intervals alternating with silty mud and clayey mud. All lithologies are structureless to slightly bioturbated and very dark gray in color, but the mud layers tend to be more brownish. Contacts are typically gradational, but a few mud layers exhibit sharp bases. Color banding is rare, and black iron-monosulfide pods are only scarcely present in some sections throughout Subunit IB. Sandy pods, probably burrows, composed of dark gray, gray, and olive gray sediment are scattered throughout. Quartz, feldspar, and accessory minerals dominate the coarse fraction. The inorganic carbonate particle content varies from 1% to 12% (Fig. 2).

The subunit is primarily distinguished by a relatively low dropstone abundance accompanied by the absence of biocarbonate and the presence of biosilica. The number of dropstones varies from 0 to 11 per core (Fig. 3). The diameter of the dropstones is variable and in general less than 8 cm (Fig. 4), but one dropstone located at 70.6 mbsf has a thickness of 28 cm (Fig. 6). This dropstone is a sandstone, with mm-scale lamination of varying frequency and cross-stratified laminae. The darker laminae consist of compacted aggregates of clay-sized material, rich in organic matter. The coarse fraction (~80% of the grains) is dominated by quartz and feldspar in a carbonate cement. Sandstones and siltstones are the predominant type of dropstones throughout. Igneous and metamorphic rocks are rare compared to Subunit IA (Table 2). Smear-slide data reveal up to 2% siliceous microfossils (diatoms and spicules) in this subunit, concentrated between 80 and 130 mbsf and below 189 mbsf.

Interpretation

The recovered sediments suggest a hemipelagic, glacial-marine depositional environment characterized by a large input of silt- to sand-sized siliciclastics. The input of siliciclastics has varied through time, but no major trends are recorded in the sequence (Fig. 2). Because of the relatively shallow water depth (1040 m) and the location on the southern Yermak Plateau, several transport modes for siliciclastic particles are possible. The siliciclastics can be deposited by melting icebergs, from sea ice, or by downslope sediment transport and redeposition. Three observations indicate that the coarser material generally was not deposited by downslope sediment transport: (1) dropstones were observed in all lithologies, (2) coarse- and fine-grained lithologies have similar particle composition, and (3) no clear evidence is found for sedimentary structures indicative of gravity

Table 2. Occurrences of dropstones at Site 912.

Core, section, interval top (cm)	Depth (mbsf)	Size (cm)	Lithology
151-912A-			
1H-2, 20	1.70	1.2	Igneous
1H-3, 36	3.36	2.0	Siltstone
2H-1, 21	4.21	2.9	Plutonic
2H-1, 21	4.21	1.3	Plutonic
2H-1, 118	5.18	1.3	Quartz
2H-1, 132	5.32	1.6	Plutonic
2H-2, 18	5.68	3.2	Sandstone
2H-3, 105	8.05	2.5	Siltstone
2H-3, 133	8.33	1.2	Igneous
2H-3, 133	8.33	2.0	Mudstone
2H-4, 64	9.14	1.4	Plutonic
2H-4, 80	9.30	2.4	Sandstone
2H-4, 110	9.60	1.7	Siltstone
2H-4, 136	9.86	1.3	Sandstone
2H-5, 16	10.16	1.2	Mudstone
2H-5, 25	10.25	3.2	Mudstone
2H-5, 25	10.25	1.6	Sandstone
2H-5, 114	11.14	1.3	Coal
2H-6, 2	11.52	1.5	Sandstone
2H-6, 17	11.67	3.0	Metamorphic
2H-6, 24	11.74	1.5	Mudstone
2H-6, 52	12.02	2.5	Sandstone
2H-6, 70	12.20	5.5	Siltstone
2H-CC, 15	13.78	2.0	Shale
3H-1, 18	13.68	2.0	Chert
3H-1, 21	13.71	1.7	Limestone
3H-1, 74	14.24	1.9	Quartz
3H-1, 84	14.34	1.7	Siltstone
3H-1, 101	14.51	1.0	Calcareous siltstone
3H-1, 127	14.77	1.0	Shale
3H-2, 34	15.34	1.5	Siltstone
3H-2, 66	15.66	1.3	Siltstone
3H-2, 136	16.36	2.1	Siltstone
3H-3, 10	16.60	1.9	Quartzite
3H-3, 10	16.60	1.6	Shale
3H-3, 135	17.85	5.0	Sandstone
3H-4, 47	18.47	1.0	Siltstone
3H-5, 66	20.16	1.0	Siltstone
3H-5, 136	20.92	2.5	Sandstone
3H-6, 87	21.87	1.3	Calcareous sandstone
3H-7, 47	22.97	1.7	Igneous
4H-1, 86	23.86	1.0	Carbonate
4H-1, 92	23.92	2.0	Sandstone
4H-2, 7	24.57	3.0	Schist
4H-2, 23	24.73	2.0	Slate
4H-2, 29	24.79	2.5	Metamorphic
4H-2, 102	25.52	1.0	Mudstone
4H-2, 137	25.87	2.0	Mudstone
4H-2, 146	25.96	1.0	Mudstone
4H-3, 33	26.33	2.7	Quartzite
4H-3, 48	26.48	1.0	Plutonic
4H-3, 48	26.48	1.0	Sandstone
4H-3, 104	27.04	1.3	Pyritic sedimentary
4H-4, 16	27.66	1.8	Plutonic
4H-4, 19	27.69	1.5	Sandstone
4H-4, 20	27.70	1.7	Coal
4H-4, 67	28.17	1.2	Sandstone
4H-5, 51	29.51	1.1	Sandstone
4H-5, 99	29.99	1.0	Mudstone
4H-5, 140	30.40	2.4	Metamorphic
4H-5, 140	30.40	2.2	Metamorphic
4H-5, 140	30.40	2.0	Metamorphic
4H-6, 52	31.02	1.0	Metamorphic
4H-6, 60	31.10	1.0	Metamorphic
4H-6, 66	31.16	3.1	Metamorphic
5H-1, 5	32.55	2.5	Siltstone
5H-1, 5	32.55	1.3	Siltstone
5H-1, 5	32.55	1.0	Siltstone
5H-1, 70	33.20	1.1	Mudstone
5H-1, 131	33.81	2.8	Sandstone
5H-1, 134	33.84	2.6	Mudstone
5H-1, 134	33.84	1.3	Sandstone
5H-2, 55	34.55	1.5	Siltstone
5H-2, 93	34.93	1.5	Siltstone
5H-4, 10	37.10	2.5	Siltstone
5H-4, 117	38.17	3.0	Phyllite
5H-5, 27	38.77	2.5	Siltstone
5H-5, 141	39.91	1.4	Limestone
5H-7, 45	41.95	2.5	Siltstone
6H-1, 120	43.20	2.0	Siltstone
6H-1, 121	43.21	1.5	Siltstone
6H-2, 50	44.00	5.9	Siltstone
6H-3, 108	46.08	2.5	Siltstone
6H-4, 34	46.84	1.0	Siltstone
6H-4, 47	46.97	1.5	Siltstone
6H-6, 73	50.23	1.0	Quartzite
6H-7, 76	51.76	1.0	Quartzite
7H-1, 32	51.82	1.6	Phyllite
7H-1, 40	51.90	1.5	Quartzite
7H-4, 8	56.08	6.5	Shale
7H-4, 93	56.93	1.6	Phyllite
7H-5, 109	58.59	1.0	Dolostone
7H-6, 23	59.23	1.2	Shale
7H-6, 57	59.57	1.2	Siltstone
7H-6, 70	59.70	1.8	Siltstone
7H-7, 60	61.10	4.5	Slate
7H-CC, 13	61.47	4.0	Siltstone
7H-CC, 30	61.64	4.5	Limestone
8H-2, 120	63.70	1.1	Sandstone
8H-3, 95	64.95	1.5	Sandstone
8H-4, 29	65.79	3.5	Sandstone
8H-4, 76	66.26	1.6	Sandstone
8H-6, 42	68.92	3.7	Sandstone
8H-6, 114	69.64	1.2	Shale
9X-1, 8	70.58	28.0	Sandstone
9X-1, 72	71.22	2.2	Sandstone
9X-3, 20	73.70	1.2	Sandstone
9X-3, 75	74.25	1.3	Sandstone
10X-3, 14	81.14	5.0	Sandstone
10X-3, 125	82.25	2.0	Siltstone
10X-3, 136	82.36	1.0	Chert
11X-1, 47	88.07	3.0	Coal
11X-1, 66	88.26	1.2	Feldspar
11X-2, 54	90.04	1.3	Schist
11X-2, 131	90.41	2.0	Chert
11X-3, 105	91.65	2.5	Siltstone
11X-3, 120	91.80	3.2	Sandstone
11X-6, 37	95.47	2.0	Granite
11X-6, 72	95.82	1.0	Phyllite
11X-6, 112	96.22	1.2	Mudstone
11X-7, 2	96.43	1.3	Mudstone
13X-1, 122	108.12	2.6	Shale
15X-1, 136	127.46	1.6	Limestone
15X-2, 106	128.58	1.2	Sandstone
16X-1, 5	135.85	7.0	Dolostone
16X-1, 10	135.90	8.0	Sandstone
151-912B-			
1H-1, 92	0.92	2.5	Plutonic
1H-2, 12	1.62	1.7	Plutonic
1H-2, 63	2.13	1.3	Siltstone
1H-2, 65	2.15	1.4	Siltstone
1H-2, 70	2.20	1.9	Siltstone
1H-2, 150	3.00	1.0	Sandstone
1H-3, 5	3.05	1.0	Feldspar
1H-3, 22	3.22	1.3	Schist
1H-3, 22	3.22	1.5	Siltstone
1H-3, 34	3.34	2.2	Sandstone
2H-2, 140	8.20	2.9	Siltstone
2H-3, 21	8.51	1.1	Quartzite
2H-3, 24	8.54	2.7	Siltstone
2H-3, 57	8.87	2.1	Siltstone
2H-3, 113	9.43	2.4	Siltstone
2H-4, 25	10.05	3.2	Sandstone
2H-5, 11	11.41	1.5	Metamorphic
2H-5, 45	11.75	1.5	Quartzite
2H-5, 55	11.85	1.0	Siltstone
2H-5, 64	11.94	1.5	Quartzite
2H-5, 93	12.23	2.5	Siltstone
2H-6, 47	13.27	1.0	Siltstone
2H-6, 108	13.88	1.3	Coal
2H-6, 140	14.20	1.5	Siltstone
2H-7, 46	14.76	4.5	Siltstone
3H-1, 30	15.10	3.0	Gneiss
3H-1, 53	15.33	1.0	Carbonate
3H-1, 129	16.09	2.5	Sandstone
3H-1, 147	16.27	2.0	Siltstone
3H-2, 4	16.34	2.0	Carbonate
3H-2, 22	16.52	1.5	Mudstone
3H-2, 39	16.69	1.0	Shale
3H-3, 145	19.25	2.0	Siltstone
3H-4, 123	20.53	1.0	Siltstone
3H-4, 136	20.66	1.0	Siltstone
3H-5, 9	20.89	1.0	Siltstone
3H-5, 38	21.18	1.0	Siltstone
3H-5, 86	21.66	1.5	Metamorphic
3H-5, 131	22.11	1.0	Siltstone
3H-6, 58	22.88	1.0	Siltstone
3H-6, 99	23.29	1.0	Siltstone
3H-7, 19	23.99	1.0	Metamorphic
3H-7, 24	24.04	1.0	Siltstone
3H-7, 39	24.19	1.0	Metamorphic
3H-7, 51	24.31	1.0	Siltstone
3H-7, 51	24.31	2.0	Siltstone
4H-2, 25	26.05	1.2	Gneiss
4H-2, 33	26.13	6.3	Sandstone
4H-2, 40	26.20	3.1	Sandstone

Table 2 (continued).

Core, section, interval top (cm)	Depth (mbsf)	Size (cm)	Lithology
4H-2, 57	26.37	1.0	?
4H-2, 98	26.78	2.6	Sandstone
4H-2, 122	27.02	2.3	Sandstone
4H-2, 139	27.19	1.1	Sandstone
4H-2, 142	27.22	2.4	Slate
4H-3, 2	27.32	3.5	Gneiss
4H-3, 14	27.44	6.5	Sandstone
4H-3, 21	27.51	3.8	Sandstone
4H-3, 25	27.55	1.4	Feldspar
4H-3, 27	27.57	1.2	Siltstone
4H-3, 34	27.64	1.2	Sandstone
4H-3, 41	27.71	1.2	Schist
4H-3, 52	27.82	1.4	?
4H-3, 69	27.99	1.7	Sandstone
4H-3, 90	28.20	1.0	Feldspar
4H-3, 138	28.68	1.6	Gneiss
4H-4, 7	28.87	1.5	Siltstone
4H-4, 11	28.91	1.0	Basalt?
4H-4, 37	29.17	4.5	Siltstone
4H-4, 50	29.30	1.0	Siltstone
4H-4, 50	29.30	1.0	Siltstone
4H-4, 59	29.39	1.0	Siltstone
4H-4, 70	29.50	1.0	Siltstone
4H-4, 94	29.74	1.5	Siltstone
4H-4, 139	30.19	1.0	Siltstone
5H-1, 85	30.85	1.6	Sandstone
5H-1, 94	30.94	1.2	Siltstone
5H-2, 8	31.58	1.0	Siltstone
5H-2, 10	31.60	1.2	Sandstone
5H-3, 28	33.28	2.0	Siltstone
5H-3, 45	33.45	1.1	Sandstone
5H-3, 83	33.83	1.0	Siltstone
5H-3, 135	34.35	2.5	Sandstone
5H-4, 53	35.03	1.1	Quartzite
5H-4, 54	35.04	2.1	Sandstone
5H-4, 56	35.06	2.4	Sandstone
5H-4, 62	35.12	3.1	Chert
5H-4, 132	35.82	2.5	Quartzite
5H-4, 144	35.94	2.8	Siltstone
5H-5, 84	36.84	1.0	Siltstone
5H-5, 89	36.89	1.0	Siltstone
5H-5, 108	37.08	2.5	Siltstone
5H-5, 124	37.24	2.5	Siltstone
5H-7, 51	39.51	1.0	?

flows, contourites, or current-related deposition. Thus, we consider the siliciclastic material to be deposited by melting icebergs and sea ice. The dropstones are interpreted as deposited primarily from icebergs, because sea ice incorporates sand- and gravel-sized material only when formed near shore (Drewry, 1986).

The uphole increase in dropstone abundance at about 40 mbsf (Fig. 3) indicates an enhancement of glacially derived sediment transport, which could be related to an intensification of the Northern Hemisphere glaciations. The increases are mainly interpreted as increases in transport and melting of icebergs in the area. The minor difference in dropstone lithology between the subunits may indicate slight changes in ice circulation and source areas.

In the upper Quaternary, the number of dropstones per core is about twice as high at this site as at Sites 910 and 911 on the inner Yermak Plateau. All three sites are located at almost the same distance from Svalbard, so this difference cannot be attributed to differences in distance from source areas. Instead it could indicate that Site 912 was located closer to a major iceberg trajectory. The southern part of the Yermak Plateau might be more influenced by the East Greenland Current, which transports icebergs southward from the Arctic Ocean (Thiede et al., 1990a). If Site 912 were located close to the front between polar and North Atlantic water masses along which melting of icebergs occur, this could explain enhanced ice-rafted debris (IRD) deposition at this site.

In Subunit IA (0–40 mbsf) distinctive color banding is present in silty clay. Typically the color banding cannot be correlated to grain size, which makes a diagenetic origin most plausible. However, some minor changes in color and lithology could possibly be attributed to variations in climate. This is supported by the fact that the highest abundances of calcareous microfossils (2%–6% of total sediment) are restricted to four dark gray carbonate mud layers, although the abundance is too low to clearly indicate interglacial deposits.

The low content of microfossils in the sediment could have resulted from a combination of any of the following processes: (1) low productivity, (2) removal by dissolution or bottom currents, (3) recrystallization, and (4) dilution by siliciclastic material. Low productivity related to extensive sea-ice cover and dilution by siliciclastics are plausible explanations, whereas the amount of carbonate dissolution and recrystallization is more uncertain and difficult to test. Inorganic carbonate particles are a minor component in all lithologies (Fig. 2). One possible origin is recrystallization of calcareous nannofossils, which is supported by the presence of high abundances of inorganic carbonate particles in the layers marked by 2%–6% calcareous microfossils. However, at this site the inorganic carbonate is more irregular in shape and size and often found in mud layers, which supports ice-rafting as a depositional mechanism for at least some of the carbonate grains.

The presence of iron-monosulfide throughout the sequence indicates strongly reducing conditions in the sediments. This corresponds to a high content of sedimentary organic matter (see "Organic Geochemistry" section, this chapter). Bioturbation gives evidence for enough O_2 near the sediment-water interface to support benthic life. Bioturbation is most pronounced in Subunit IA, which may indicate increasing O_2 levels in the bottom water during the Quaternary.

BIOSTRATIGRAPHY

Introduction

A Quaternary and Pliocene sequence of ice-rafted sediments with scattered occurrences of calcareous microfossils was recovered from three holes at Site 912. Figure 7 summarizes biostratigraphic results. Siliceous microfossils are absent, with the exception of rare reworked diatoms and silicoflagellates, and rare and poorly preserved radiolarians. In Sample 151-912A-13X-CC, there are rare diatoms indicative of the uppermost Pliocene to lower upper Quaternary. Dinoflagellates are rare and non-age-diagnostic, whereas terrestrial pollen and spores are common throughout. Ice-rafted *Inoceramus* prisms (Cre-

Table 3. Summary of lithologic subunits, Site 912.

Subunit	Dominant lithology	Interval, mbsf (thickness, m)	Age	Occurrence (hole-core-section)
IA	Predominantly silty clay with intervals of clayey mud. Defined by high abundances of dropstones (10–28 per core).	0–40.0 (40.0)	Quaternary	912A-1H-1 to 5H-5, 150 cm 912B-1H-1 to 5H-CC
IB	Predominantly silty clay and clayey silt with intervals of silty mud and clayey mud. Defined by low abundances of dropstones (0–11 per core).	40.0–209.1 (169.1)	Pliocene to Quaternary	912A-5H-6, 0 cm to 16H-1 912C-1R-1 to 12R-3

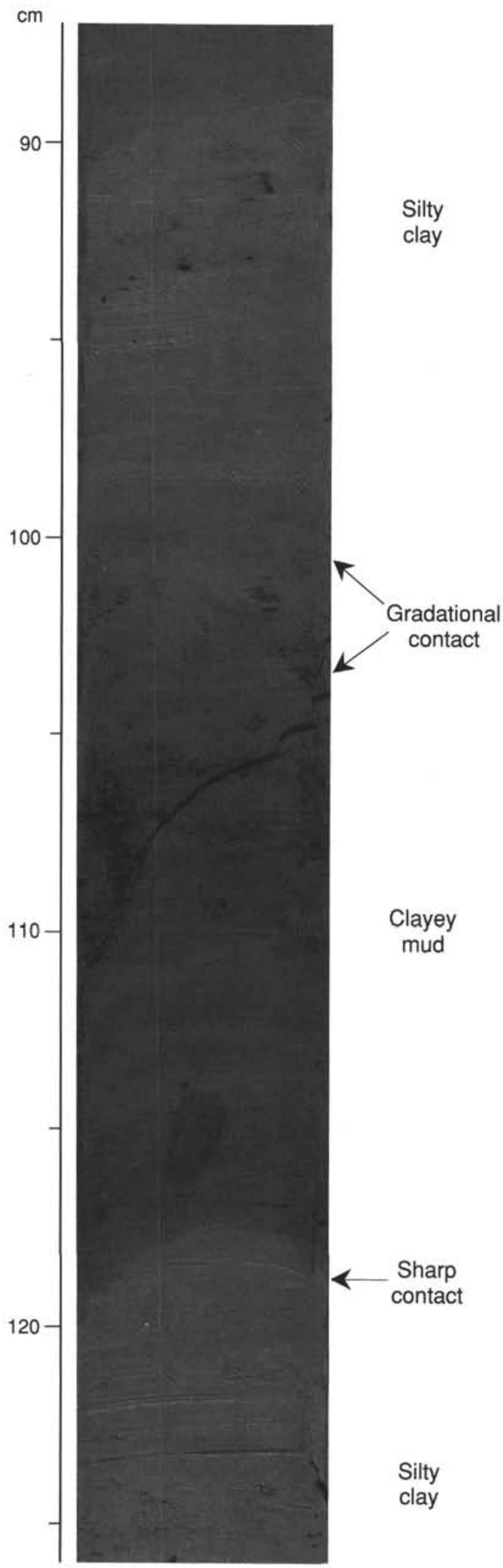

Figure 5. Example from Section 151-912B-1H-3 of alternating layers of dark gray silty clay and very dark gray clayey mud. The clayey mud layer exhibits a sharp base (117–118 cm) and a gradational, bioturbated upper contact (101–104 cm).

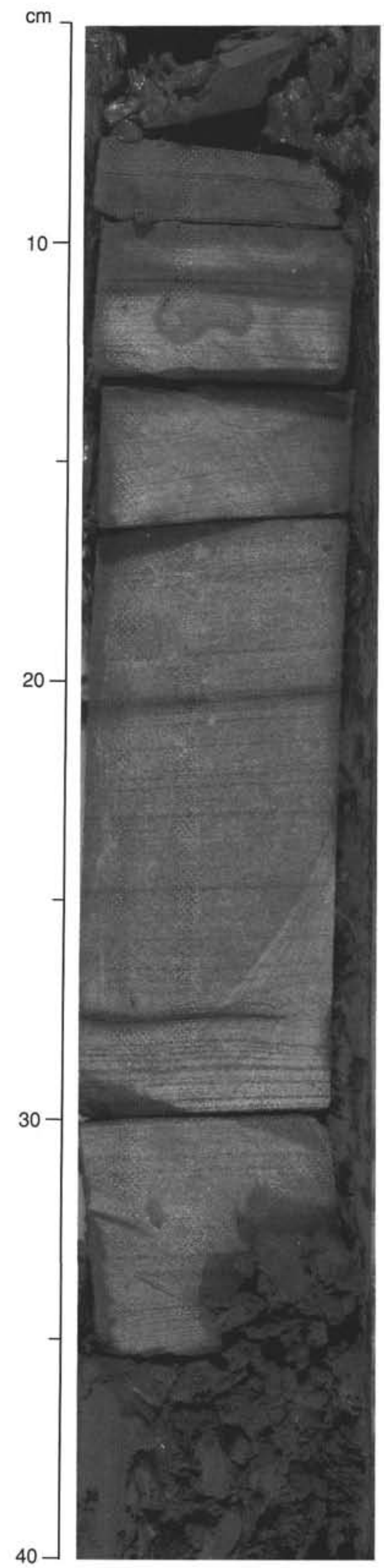

Figure 6. Close-up of a large laminated sandstone (dropstone) found at 70.6 mbsf (151-912A-9X-1, 8–35 cm). The black laminae consist of compacted, black, clay-sized particles rich in organic matter. Cross-stratified laminae are present between 33 and 35 cm, and a water-release or load structure can be seen at ~14 cm.

taceous) are found in Samples 151-912C-4R-CC through -11R-CC in Pliocene sediments.

Diatoms

Core-catcher and shipboard samples from Cores 151-912A-1H through -8H are barren of diatoms, as are all core catchers from Hole 909B (Cores 1H through 5H). Samples 151-912A-9X-CC (78.0 mbsf) and -10X-CC (87.6 mbsf) contain rare reworked diatoms, including Eocene and upper Oligocene to Miocene forms. Sample 151-912A-13X-CC (126.1 mbsf) contains reworked forms, as above, but also contains diatoms that may be in situ. These include few specimens of *Thalassiosira oestrupii, T. nidulus, Proboscia barboi,* and *Actinocyclus occulatus,* which suggest the *P. barboi* Zone of Schrader and Fenner (1976), upper upper Pliocene to lower upper Quaternary according to some correlations (Baldauf, 1984; 1987), although the age of the *P. barboi* Zone/*T. oestrupii* Zone transition is not well established. Schrader and Fenner (1976) suggest the boundary is in the upper Pliocene. The diatom assemblage at Site 907 seems to support a Pliocene age for this zonal boundary.

In addition to the above taxa, diatoms of the Pliocene *T. kryophila* Zone occur in Sample 151-912A-13X-CC, including single specimens of *T. convexa, Thalassiosira* aff. *T. complicata, T. zabellinae, Stephanopyxis horridus,* and *Stephanogonium hanzawae.* These taxa are interpreted as reworked from older Pliocene strata. Older reworked diatoms in Sample 151-912A-13X-CC include the upper Oligocene to lower Miocene marker *Rocella praenitida* and numerous long-ranging taxa.

The interpretation of *P. barboi* Zone in Core 151-912A-13X is in general agreement with calcareous nannofossils and planktonic foraminifers, which suggest the Pliocene/Quaternary boundary in Core 151-912A-15X-CC (135.8 mbsf) (Fig. 7), unless further studies provide clear evidence that the *P. barboi* Zone/*T. oestrupii* Zone transition is in the Pliocene. There was no recovery in Cores 151-912A-12X and -14X, and Cores 151-912A-15X and -16X are barren of diatoms.

Continuous rotary coring in Hole 912C began at 93.5 mbsf, although recovery throughout the cored interval was very poor. The interval containing diatoms of the *P. barboi* Zone, in Core 151-912A-13X (106.9–116.5 mbsf) is not recognized in Hole 912C, probably because of the poor recovery in this interval. Cores 151-912C-1R and 151-912C-5R through -11R are barren of diatoms. Cores 151-912C-2R through -4R contain rare, presumably reworked non-age-diagnostic diatoms. Core 151-912C-12R, including Samples 151-912C-12R-1, 30–32 cm, 151-912C-12R-1, 99–100 cm, and 151-912C-12R-CC (209.1 mbsf), contains rare to few diatoms, all of which may be reworked. The assemblage in Core 151-912C-12R includes several specimens of the lower Eocene diatom *Trinacria exculpta* and one specimen of *T. simulacrum,* as well as numerous long-ranging heavily silicified taxa.

Silicoflagellates

Rare reworked Eocene to Miocene silicoflagellates and unidentifiable silicoflagellate fragments occur in all samples from Site 912 that contain reworked diatoms (see previous "Diatoms" section). Sample 151-912A-13X-CC contains *Mesocena* cf. *M. elliptica, Naviculopsis* sp., *Dictyocha fischeri*(?), and *Corbisema tricantha.* Sample 151-912C-12R-CC contains *C. tricantha, D. deflandrei,* and *D. frenguellii.*

Radiolarians

Radiolarians recovered from core-catcher samples at Site 912 are rare, poorly preserved, and predominantly non-age-diagnostic. The recrystallized assemblage recovered from all three holes at this site

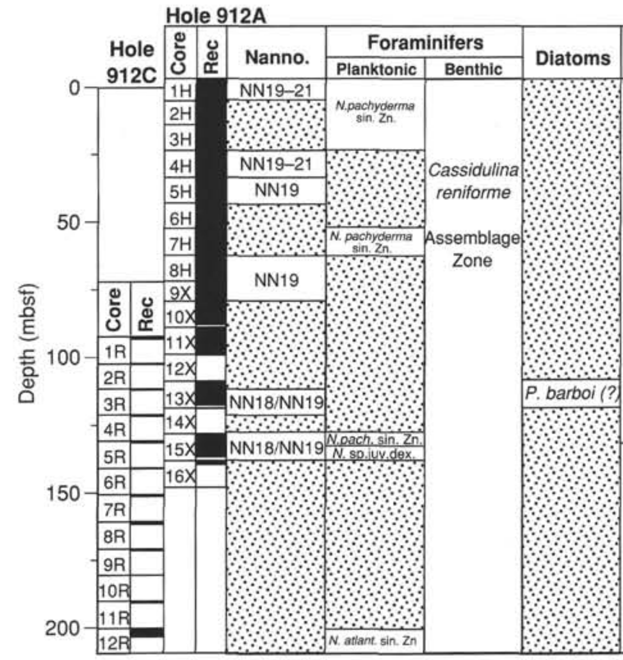

Figure 7. Summary of biostratigraphy of Site 912.

includes unidentifiable species of the genera *Spongotrochus, Spongodiscus, Stylodictya, Prunopyle, Porodiscus,* and *Actinomma.* One species, *Actinomma livae,* which ranges from the early Miocene to the Quaternary, is present in Sample 151-912C-3R-CC (122.4 mbsf). The single siliceous interval recovered from this site (Core 151-912A-13X-CC; 116.5 mbsf), which contains reworked and in-situ diatoms of the *P. barboi* Zone, has only rare, broken fragments of radiolarians, which provide no additional age control. Reworked Cretaceous radiolarians of the genera *Dictyomitra* and *Myllocerion* occur in Sample 151-912A-15X-CC (135.8 mbsf).

Calcareous Nannofossils

Moderately to poorly preserved calcareous nannofossil assemblages were analyzed in samples from Holes 912A, 912B, and 912C. Although the species diversity is low, age-diagnostic species were found in these samples.

Samples 151-912A-1H-CC and -4H-CC contain *Gephyrocapsa* sp. (small), which indicate uppermost Pliocene to Quaternary. Samples 151-912A-5H-CC through -9X-CC are characterized by the occurrence of *Pseudoemiliania lacunosa, Gephyrocapsa caribbeanica,* and *G. oceanica.* Among these samples, large *Gephyrocapsa* (>6 μm) are found in Samples 151-912A-8H-CC and -9X-CC. On the basis of these assemblages, Samples 151-912A-1H-CC through -4H-CC are correlated to upper Quaternary NN19 to NN21 Zones. Samples 151-912A-5H-CC through -9X-CC are assigned to Quaternary Zone NN19 based on the co-occurrence of *G. caribbeanica* with *P. lacunosa.* Furthermore, the occurrence of large *Gephyrocapsa* in both Samples 151-912A-8H-CC and -9X-CC indicates an age between the Cobb Mountain Event and Olduvai Event in the Matuyama Reversed Subchron (between datums 8 and 10 of Sato et al., 1991). Below Sample 151-912A-9X-CC, calcareous nannofossil assemblages are characterized by the presence of small *Gephyrocapsa, Crenalithus doronicoides,* and *Coccolithus pelagicus* and the absence of *G. caribbeanica* and *G. oceanica.* This indicates that Core 151-912A-15X lies between datums 12 and 14 (Sato et al., 1991), in or just below the Olduvai Subchron (uppermost Pliocene; NN18 to NN19 Zones).

Calcareous nannofossils occur in only one sample (151-912B-3H-CC) among five core-catcher samples from Hole 912B, and consist of poorly preserved and rare specimens of *Gephyrocapsa* sp. and *G. caribbeanica*. This indicates that the sample is correlated to the Quaternary NN19 to NN21 Zones. Nannofossils are also rare to absent in Hole 912C except in Sample 151-912C-3R-CC (122.4 mbsf), which contains small (<6 μm) *Gephyrocapsa* and no *G. caribbeanica* or *G. oceanica*. This sample is therefore correlated to the interval between datums 12 and 14 (Sato et al., 1991), near or in the Olduvai Event (nannofossil zones NN18 to NN19).

Planktonic Foraminifers

Planktonic foraminifer biostratigraphy of Site 912 is based on the examination of all core-catcher samples from Holes 912A, 912B, and 912C. Additional samples were analyzed from Cores 151-912A-15X and 151-912C-12X. Planktonic foraminifers are abundant in the upper sequence of the Quaternary sediments and occur sporadically in the downhole sequence. All core-catcher samples from Hole 909C, except Sample 151-912C-12X-3, were barren of planktonic foraminifers.

Planktonic foraminifers at Site 912 are well preserved. Monospecific *Neogloboquadrina pachyderma* sin. assemblages indicate an age of Quaternary for Cores 151-912A-1H through -3H, and 151-912B-1H through -4H. Core-catcher samples from Cores 151-912A-4H through -16X are barren with the exception of a single specimen of *N. pachyderma* in Sample 151-912A-7H-CC. Cores 151-912A-12X and -14X have no recovery. Six additional samples from Core 151-912A-15X were processed to define the boundary between the Quaternary and the Pliocene. Samples from Sections 151-912A-15X-1, -2 and -4 are barren. Samples from Sections -15X-3 and -15X-5 contain *N. pachyderma* sin., indicating Quaternary. Sample 151-912A-15X-5, 33–37 cm, has the dextral coiling juvenile *Neogloboquadrina*, similar to the sequence observed at Site 910, where they indicate uppermost Pliocene. Samples 151-912A-15X-CC and -16X-CC are barren. In the lowermost part of the sequence at Site 912, planktonic foraminifers from Core 151-912C-12R indicate the presence of the Pliocene *N. atlantica* sin. Zone.

Benthic Foraminifers

Benthic foraminifers were examined in core-catcher samples from Holes 912A and 912C. Most samples contain rare benthic foraminifers, but several samples contain abundant specimens. Overall, only one zone appears to occur at this site, although the assemblage changes slightly. The intervals below Sample 151-912A-9X-CC and Sample 151-912C-12R-CC are dominated by *Cassidulina reniforme*, whereas the upper part of each hole is characterized by abundant *C. laevigata* and *C. teretis*. *C. reniforme* prefers shallower water than do the other two species. This suggests a change in water depth in the earlier depositional history of Site 912.

Palynology

All core-catcher samples from Hole 912C were processed for palynology. All samples contain abundant plant debris, amorphous organic matter, and common terrestrial pollen and spores. Dinoflagellate cysts are rare and are either non-age-diagnostic or reworked older taxa.

Biostratigraphic Synthesis

The sequence recovered at Site 912 ranges from Quaternary to Pliocene, based on intermittent occurrences of planktonic foraminifers and calcareous nannofossils. The Quaternary is recognized by nannofossil zones NN21 to NN19 from Core 151-912A-1H down to Core 151-912A-9X, and by the planktonic foraminifer *N. pachyderma* sin. Zone down to Section 151-912A-15X-5. Juvenile dextrally coiled specimens of *Neogloboquadrina* in Sample 151-912A-15X-5, 33–37 cm, may indicate the top of the Pliocene, based on comparison with the planktonic foraminifer assemblages at nearby Site 910. The deepest core at Site 912, Core 151-912C-12R, contains the *N. atlantica* sin. Zone, indicative of Pliocene age. A diatom assemblage indicative of the *P. barboi* Zone in Core 151-912A-13X provides an age of latest Pliocene to early late Quaternary, in agreement with the calcareous microfossil ages. A change in the benthic foraminifer assemblage at about Core 151-912A-9X suggests a change from shallower water depths below this level to deeper water depths above this level.

PALEOMAGNETICS

Shipboard paleomagnetic studies performed at Site 912 followed the general methods described in the "Explanatory Notes" chapter (this volume). Paleomagnetic studies provided significant temporal constraints for the sedimentary column with the identification of major chronozones and several short subchronozones. Rock magnetic studies were undertaken at this site to determine the nature of these ferromagnetic iron sulfide concretions and the role they played in the magnetic properties.

General Magnetic Character of the Site 912 Sediments

As in other sites from the Yermak Plateau, secondary magnetizations acquired by diagenetic iron sulfides may play a large role in the natural remanent magnetization (NRM) measured in Site 912 cores. The NRM after a 30-mT demagnetization and the magnetic susceptibility measured on the MST system show generally low values, except in occasional thin intervals in which the two quantities peak 10 or 100 times above background (Fig. 8). NRM intensity after 30-mT demagnetization treatment shows a similar distribution, with a median value of intensity at about 2.7×10^{-3} Am^{-1}. As was noted at Sites 910 and 911, visual inspection of the core shows that these high susceptibility peaks are often associated with iron sulfide concretions. Besides these occasional spikes in magnetic properties, the susceptibility and NRM after 30-mT AF demagnetization show sharp decreases (by a factor of about 2) below 16 mbsf (Fig. 8). A similar decrease is not observed in GRAPE density, thus the drop in susceptibility is probably not a result of core disturbance. We think this feature reflects true variation in the rock magnetic properties of the sediment because a similar offset, at the same depth, is observed in Hole 912B as well (Fig. 9). This offset creates a bimodal distribution in magnetic susceptibility; sediments below 15.5 mbsf have a median value of about 1.7×10^{-4} SI units, whereas the susceptibilities of sediments above 15.5 mbsf cluster around 4×10^{-4} SI units. In addition to these two elements, the very spiky iron sulfide signal is reflected in this distribution as a slender tail toward higher values (Fig. 10). This discontinuity coincides with the boundary between a near surface (0–15.5 mbsf) oxidized zone, which is characterized by low methane content, low total sulfur, and high sulfate in the interstitial water, and a lower (deeper than 15.5 mbsf) reduced zone with high methane content, high sulfur values, and near zero sulfate in the interstitial fluid (see Figs. 14 and 16 of the "Inorganic Geochemistry" and "Organic Geochemistry" sections, respectively, this chapter). This boundary probably represents a diagenetic alteration of iron oxides to iron monosulfides at a reaction front between downwardly transported sulfate and upwardly mobile methane. That this reaction front occurs so low in the section has important consequences for the interpretation of the magnetostratigraphy. If this represents the "lock-in depth" for the characteristic magnetization, then there would be a considerable lag between the depositional age and the age of the char-

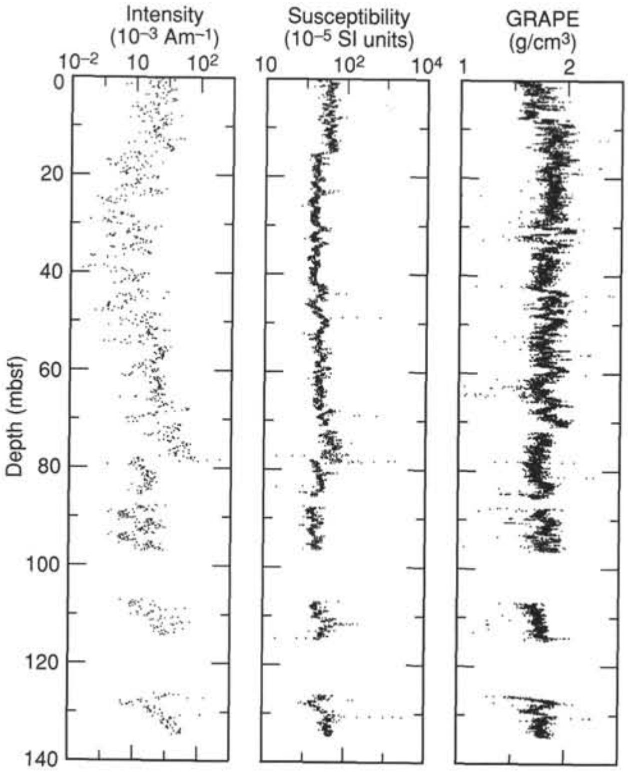

Figure 8. The variation in NRM intensity after 30-mT AF demagnetization, magnetic susceptibility, and GRAPE density with depth in Hole 912A.

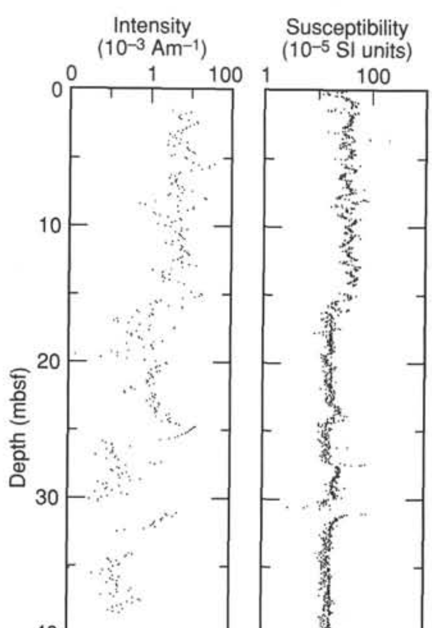

Figure 9. The variation in NRM intensity after 30-mT demagnetization treatment and magnetic susceptibility in Hole 912B.

acteristic magnetization. Further shore-based study of discrete samples from this hole should determine which magnetic phases are present and establish their importance as carriers of the magnetostratigraphic signal. A step-like discontinuity in magnetic susceptibility also is observed in Hole 912A at about 78 mbsf (Fig. 8), nearly coincident with the abrupt occurrence of silty mud in the lithostratigraphic record. In this case the discontinuity probably represents a depositional change in sediment type rather than a chemical reaction process.

AF Demagnetization Behavior and Rock Magnetism

To examine the composition of the ferromagnetic mineralogy of the sediments, a combination of saturation isothermal remanent magnetization (SIRM) and two partial anhysteretic remanent magnetizations (PARMs) was imparted to the samples along three orthogonal axes and followed by stepwise thermal demagnetization. An SIRM was applied with a pulsed field (maximum intensity = 1.2 T) along the Z axis, a PARM was applied along the Y axis in the 30-mT to 95-mT coercivity window, and a final PARM was applied along the X axis in the 0-mT to 30-mT coercivity window. In all cases the final remanence of the sample was dominated by the SIRM signal (the Z axis, see Fig. 11A). Thermal demagnetization indicated that the high coercivity mineral that dominates the remanent-carrying potential of these sediments has a very discrete unblocking temperature between 275°C and 350°C consistent with the magnetic properties of iron sulfides (Fig. 11B). A very small (<1% of the total) component of the remanence persists until it is finally unblocked between 500°C and 600°C suggesting the presence of a small amount of iron oxide.

Further shore-based work will be necessary to determine what role these complex magnetic mineral assemblages play in the characteristic magnetization of the sediments. Chemical alteration of sediments is a recognized complication in thermal demagnetization experiments; however, the small change in susceptibility during ship-based experiments indicates little chemical alteration of the magnetic minerals during thermal treatment to 600°C. Thus, further thermal demagnetization treatment is likely to be effective.

Magnetic Polarity Stratigraphy

Pass-through measurements of NRM with a 30-mT demagnetization were performed on Hole 912A archive core halves from just be-

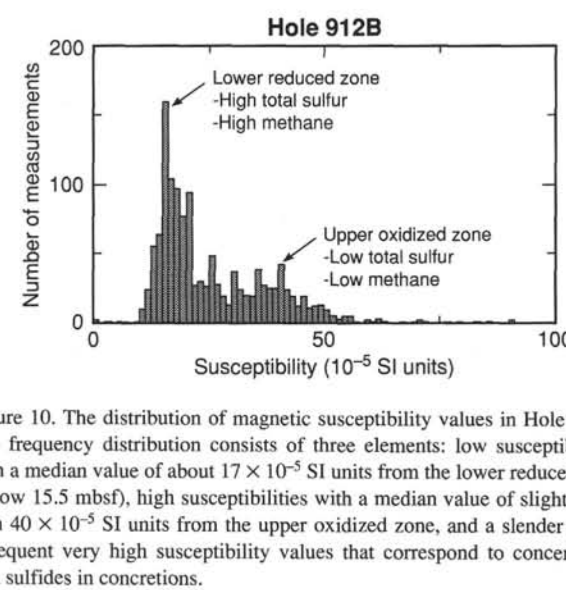

Figure 10. The distribution of magnetic susceptibility values in Hole 912B. The frequency distribution consists of three elements: low susceptibilities with a median value of about 17×10^{-5} SI units from the lower reduced zone (below 15.5 mbsf), high susceptibilities with a median value of slightly less than 40×10^{-5} SI units from the upper oxidized zone, and a slender tail of infrequent very high susceptibility values that correspond to concentrated iron sulfides in concretions.

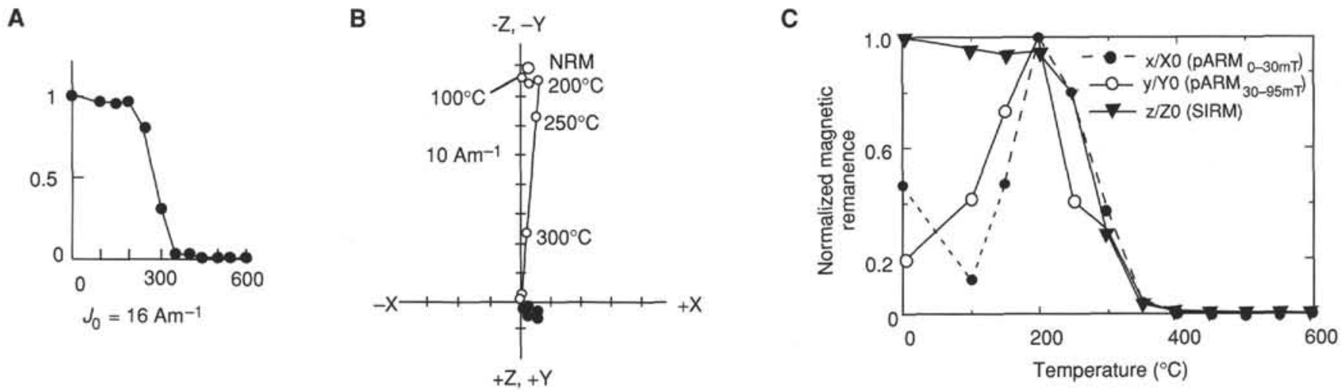

Figure 11. The results of the thermal demagnetization of composite PARMs and an SIRM applied to the x, y, and z axes of the sample (details described in the text). **A.** The variation in intensity with thermal treatment. The SIRM is unblocked in an extremely narrow temperature range consistent with the SIRM being carried by iron sulfides. **B.** Orthogonal axis demagnetogram showing thermal demagnetization of sediment from 112 mbsf in Hole 912A. Open circles are the projection of vector endpoints onto the vertical plane perpendicular to the split face of the core (xz plane). Filled circles are the projection onto the horizontal plane (xy plane). **C.** Plot showing the thermal demagnetization of each of the separate components of SIRM and PARM. Each component has been normalized to its initial, pre-heating value.

low the sediment water interface down to 135 mbsf, and on Hole 912B archive halves from just below the seafloor to a depth of 40 mbsf. Consistent inclination vs. depth records between Holes 912A and 912B in the region of their overlap support the notion that the inclinations from the two holes are reliable recorders of the geomagnetic field. In Figure 12 we propose an interpretation of the inclination record in terms of normal and reversed polarity zones. The inclination record was fairly easily interpreted for most of Holes 912A and 912B except at a depth of about 25 to 30 mbsf in both cores, where a zone of intermediate inclinations is observed. Scattered intervals of poor recovery complicate the interpretation of the magnetostratigraphy, especially in Hole 912A. Pass-through measurements on Hole 912C cores did not add significantly to the magnetostratigraphic record because of poor recovery in that hole. The magnetic polarity stratigraphy was interpreted from the inclination of the NRM after the 30-mT treatment (Fig. 12 and Table 4). In both holes the Brunhes/Matuyama (C1n/C1r) boundary is placed at the base of zones of consistently steep positive inclinations that are observed at the tops of both cores. The exact placement is complicated in both records by zones of intermediate inclinations. The Jaramillo subchronozone (C1r.1n) is observed in both holes, its top boundary being poorly defined at about 30 m. However, the lower boundary of the Jaramillo is well defined by a relatively sharp transition from steep upward to steep downward inclinations at about 35 mbsf. Below 40 mbsf, the record from Hole 912A is predominantly of reversed polarity with only three relatively thin normal-polarity magnetozones. We interpret the upper zone (54.7 to 53.8 mbsf) as the Cobb Mountain subchronozone and the lowermost zone (recorded only in Core 151-912A-13X) as the Olduvai subchronozone. Because of the near zero recovery in Cores 151-912A-12 and -14, the boundaries of the Olduvai in Table 4 are placed at the centers of these missed recovery intervals. Between about 75 and 78 mbsf we observe a fairly well defined interval of normal polarity that is difficult to reconcile with the geomagnetic polarity time scale (GPTS) of Cande and Kent (1992). The bottom of this zone is bounded by a core break; however, the upper boundary falls within Section 151-912A-9X-3, so it is difficult to explain this zone as a simple coring artifact. The reversal occurs at an abrupt change in susceptibility and NRM intensity. This is also at approximately the same depth as the sharp increase in the silt fraction and the appearance of dropstones (see "Lithostratigraphy" section, this chapter). Further shore-based study will be necessary to determine whether this magnetozone has any chronologic significance or is merely reflecting the selective remagnetization of this sediment interval.

Comparison Between Magnetostratigraphy and Biostratigraphy

Figure 13 indicates the age vs. depth relationship implied by the correlations discussed above and the GPTS of Cande and Kent (1992). According to the magnetostratigraphy, the base of the section

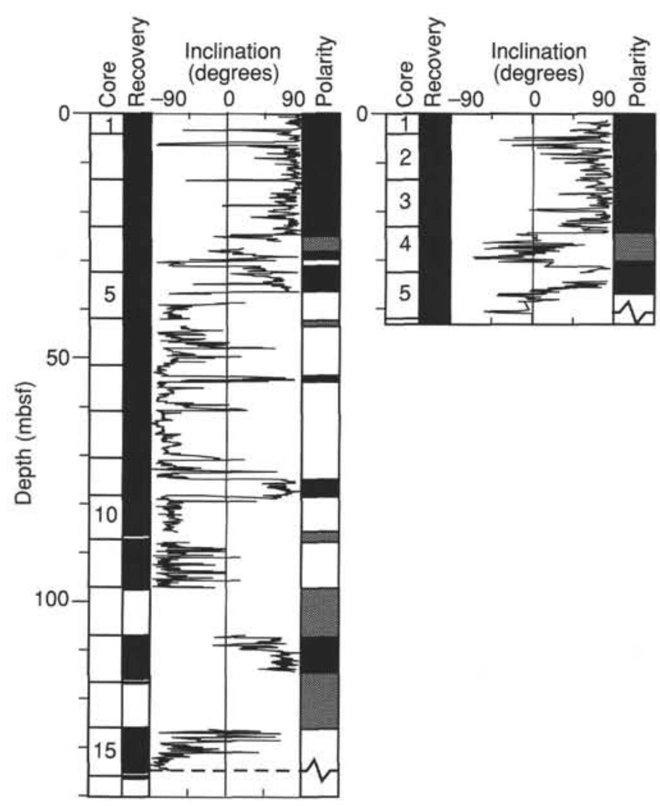

Figure 12. The paleomagnetic record from Holes 912A (left) and 912B (right). For each hole, the left columns show the cored intervals with the length of the recovered core indicated in black, the center column is the inclination of the NRM after a 30-mT AF demagnetization treatment, and the right column is the interpreted polarity. Black = normal polarity, gray = indeterminate polarity or missed recovery, and white = reversed polarity.

studied paleomagnetically in Hole 912A (135 mbsf) was deposited shortly before the Olduvai subchron at approximately 2 Ma. As discussed in the "Biostratigraphy" section (this chapter), the calcareous nannofossils are particularly age diagnostic at this locale, and the biostratigraphic ages are completely consistent with Figure 13. The occurrence of large *Gephyrocapsa* in Sections 151-912A-8H-CC and 151-912A-9X-CC (70.5 and 78 mbsf) is also consistent with the locations of the base of the Brunhes Chronozone (C1n.o at 24.6 mbsf) and the top of the Cobb Mountain subchronozone (C1r.2r-1n.t at 53.8 mbsf) in Hole 912A and the range determined for this form by Sato and Takayama (1992). Likewise, position of the nannofossil assemblage obtained from Core 151-912A-15X, just below the Olduvai subchronozone (the base of which is placed at 121.6 mbsf within the poorly recovered Core 151-912A-14X) is consistent with the observed range of important elements of this nannofossil assemblage (Sato and Takayama, 1992). Thus the Pliocene/Pleistocene boundary is placed at similar levels on both biostratigraphic and magnetostratigraphic grounds. These preliminary results indicate a relatively short time lag between depositional processes and the acquisition of the characteristic magnetization. This is surprising because of the relatively deep diagenetic front at Site 912 (15.5 mbsf). Nevertheless, the close agreement of the paleomagnetic and biostratigraphic ages suggests a more complex chemical remanence acquisition process than generally admitted in most previous paleomagnetic studies.

Table 4. Magnetozone boundaries and apparent sedimentation rates in Holes 912A and 912B.

Depth (mbsf)	Age (Ma)	Sed. rate (m/m.y.)	Chron
Hole 912A			
0	0		
		31.5	C1n
24.6	0.780		
		32.4	
31.2	0.984		
		81.5	C1r.1n
36.5	1.049		
		113.8	
53.8	1.201		
		81.8	C1r.2r-1n
54.7	1.212		
74.6	?		
			?
78	?		
107.1	1.757		
		>64.2	C2n
121.6	1.983		
Hole 912B			
0	0		
		31.2	C1n
24.3	0.78		
		28.9	
30.2	0.984		
		100.0	C1r.1n
36.7	1.049		

Note: Sedimentation rates are calculated by linear interpolation between two successive ages.

Sedimentation Rates

The poor recovery below 140 mbsf makes it impossible to estimate Pliocene sedimentation rates magnetostratigraphically. The average pre-Jaramillo sedimentation rates depend on the exact position of the Olduvai subchronozone boundaries, and vary from about 80 m/m.y. to 100 m/m.y. Apparent sedimentation rates at Site 912 decreased to about 30 m/m.y. during the last 1 m.y. of deposition (see Table 4 and Fig. 13).

Conclusions

The magnetostratigraphic results from Site 912 yield a fairly robust age vs. depth model for the sediments at this site. Poor recovery within a couple of key zones near the Brunhes/Matuyama boundary and surrounding the Olduvai subchronozone prevents an exact specification of the ages in the section. However, despite the presence of high coercive diagenetic iron sulfides in the sediment, the magnetostratigraphy is entirely consistent with the available biostratigraphic information.

INORGANIC GEOCHEMISTRY

Interstitial Water

Table 5 and Figure 14 show the composition of interstitial waters collected from Holes 912A and 912C. Sodium shows a modest dilution due to early clay diagenesis, and potassium is depleted by the same process. Magnesium decreases from the seawater value in the

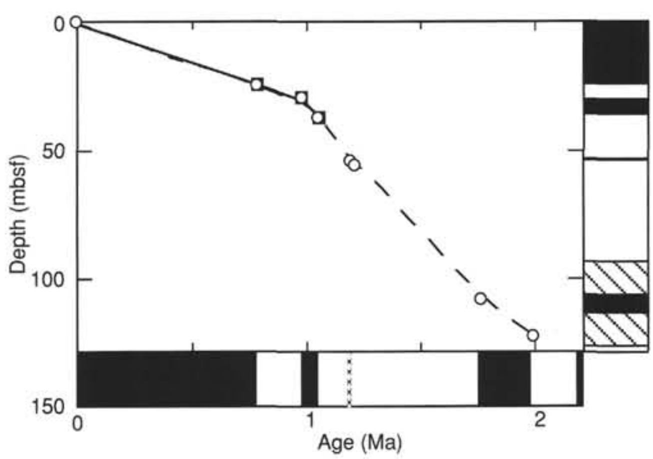

Figure 13. Age-depth model based on the magnetostratigraphy of sediments in Hole 912A (circles) and 912B (squares). There is a large uncertainty in the Olduvai subchronozone boundaries due to poor recovery in Cores 151-912A-12X and 151-912A-14X.

Table 5. Composition of interstitial waters in Holes 912A and 912C.

Core, section	Depth (mbsf)	Na (mmol/L)	K (mmol/L)	Mg (mmol/L)	Ca (mmol/L)	Cl (mmol/L)	SO_4 (mmol/L)	NH_4 (μmol/L)	SiO_2 (μmol/L)	pH	Alkalinity (meq/L)
151-912A-											
1H-2	2.95	475	13.4	51.7	10.4	542	26.4	218	192	7.44	4.451
4H-7	32.60	442	10.4	33.4	2.4	539	0.0	519	387	7.72	12.193
7H-7	61.29	418	8.5	30.0	3.1	514	0.0	1044	453	7.75	12.718
10X-4	83.95	420	8.9	26.7	3.5	509	0.0	1600	546	7.75	13.526
13X-3	111.22	427	8.5	24.5	3.9	498	0.0	2049	579	7.76	13.201
151-912C-											
12R-1										7.97	19.381

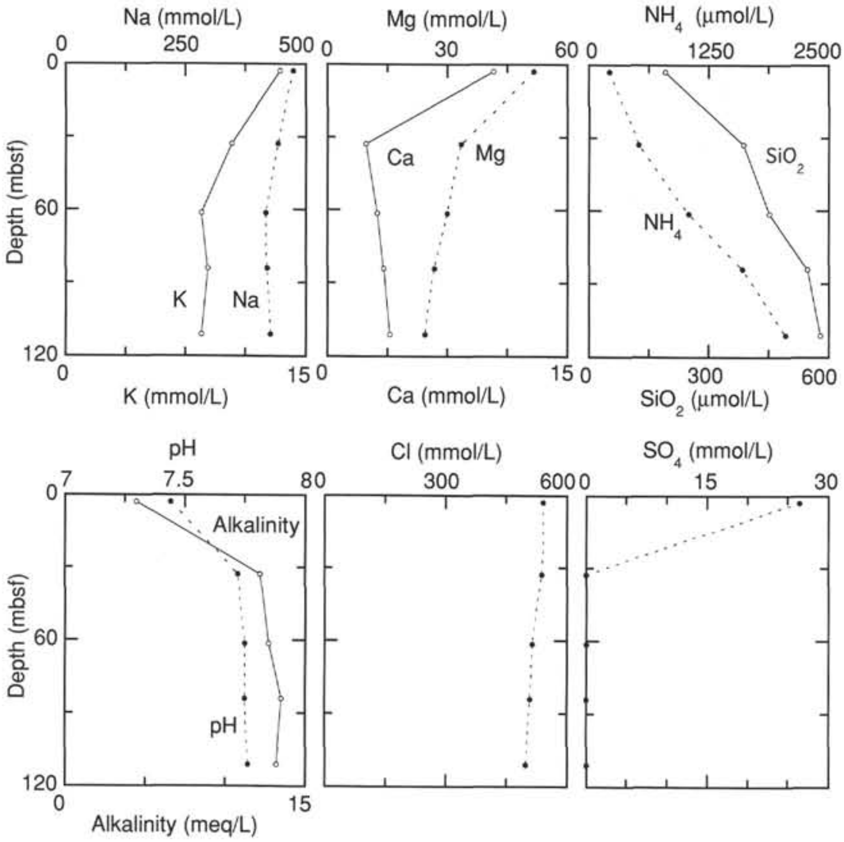

Figure 14. Interstitial water compositions at Site 912.

uppermost core sampled to about one half of that value at 100 mbsf. Calcium shows a rapid decrease from well above the level of ambient seawater in the first core samples down to the seawater value at about 30 mbsf, and then increases slowly with increasing depth.

Ammonia increases to levels above 1000 µmol/L below 100 mbsf. Silica increases to around 600 µmol/L below 100 mbsf. The general dearth of siliceous microfossils suggests that dissolved silica is controlled by the formation of opal CT and that amorphous silica has been exhausted in these sediments.

Alkalinity and pH both rise rapidly near the surface and then level off, indicating that carbonate dissolution has reached some steady state. It is worth noting that the high calcium concentration observed in these interstitial waters at the sediment-water interface is not reflected in the alkalinity or pH profiles and may reflect an unexplained artifact. It does not appear to be caused by carbonate dissolution, as alkalinity does not rise by an equivalent amount.

Chloride shows the same slight dilution effect as sodium because of the dehydration of clays. Sulfate shows a rapid decrease from seawater levels to zero below 20 mbsf, and methane (see "Organic Geochemistry" section, this chapter) becomes abundant at about the same depth.

Sediment Geochemistry

Table 6 shows major element abundances measured on samples from Holes 912A and 912C by X-ray fluorescence on pressed pellets. Silica (Fig. 15) is relatively constant in these sediments, and the average concentration, about 60 wt%, is high. TiO_2 is also constant at about 1 wt%, indicating little variation in composition caused by dilution by exotic components. Alumina and total iron (Fig. 15) similarly show little variation.

Magnesium and calcium (Fig. 15) show no major changes, although magnesium appears to decrease gradually with increasing depth in the section. Sodium and potassium (Fig. 15) also appear to show no trend, although a slight decrease in potassium below approximately 150 mbsf may signal the start of the shift to lower potassium abundances noted at other sites in the region. Unfortunately, the record is not long enough to clearly show this change.

Discussion

The chemistry of sediments at Site 912 shows only hints of variation. Potassium in the solids may be shifting to lower (preglacial?) values, but the record stops too soon to tell. Sulfate reduction is proceeding at a relatively rapid pace, and the formation of diagenetic sulfides, mostly "mono-sulfides" (greigite, mackinawite and pyrrhotite), in the upper parts of the section appears to be rapid and may contribute to the remanent magnetism.

The initial high calcium value mentioned previously appears in other cores as well and is not matched by an equivalent increase in alkalinity. This steep calcium gradient in the uppermost cores suggests the diffusion of calcium into the core tops, an unlikely process. There appears to be an artifact in the analysis of calcium in these surface cores, perhaps associated with the sulfate abundance. As yet, this artifact is unexplained.

ORGANIC GEOCHEMISTRY

The shipboard organic geochemistry program at Site 912 included analyses of volatile hydrocarbons and determinations of inorganic carbon, total nitrogen, total carbon, and total sulfur (for methods, see "Explanatory Notes" chapter, this volume).

Table 6. Major element composition of sediments in Holes 912A and 912C.

Core, section	Depth (mbsf)	SiO_2 (wt%)	TiO_2 (wt%)	Al_2O_3 (wt%)	Fe_2O_3 (wt%)	MnO (wt%)	MgO (wt%)	CaO (wt%)	Na_2O (wt%)	K_2O (wt%)	P_2O_5 (wt%)	Total (wt%)
151-912A-												
1H-3	3.63	58.99	0.88	15.75	6.50	0.04	3.19	2.10	1.96	3.34	0.29	93.03
2H-3	7.63	56.29	1.00	17.61	8.84	0.08	3.58	1.92	2.13	3.30	0.16	94.91
3H-3	17.11	60.15	0.90	15.80	6.21	0.06	3.13	2.00	2.09	2.86	0.19	93.37
4H-3	26.64	60.01	0.91	15.73	5.80	0.04	3.31	2.10	1.98	3.32	0.17	93.38
5H-3	36.10	60.29	0.95	16.15	6.86	0.05	3.38	2.04	1.99	3.37	0.15	95.22
6H-3	45.61	60.44	0.95	16.30	6.46	0.05	3.23	1.94	1.99	3.22	0.18	94.75
7H-3	55.11	59.27	0.95	16.34	8.16	0.07	3.24	1.95	2.17	3.07	0.18	95.40
8H-3	64.57	61.84	0.97	15.89	6.61	0.04	3.13	1.93	2.01	3.31	0.13	95.85
9X-3	74.14	59.28	0.89	15.84	6.94	0.06	2.79	2.30	1.80	2.90	0.63	93.44
10X-3	81.60	59.19	0.90	15.19	7.11	0.05	3.16	2.01	2.05	3.20	0.16	93.01
11X-3	89.72	61.62	0.94	15.82	6.02	0.04	2.99	1.87	2.06	2.96	0.19	94.51
13X-3	110.53	59.77	1.00	15.69	7.29	0.06	3.40	2.16	2.26	3.04	0.15	94.81
15X-3	129.28	59.45	1.01	17.28	7.96	0.07	2.90	1.82	1.92	3.05	0.17	95.63
151-912C-												
5R-CC	132.17	61.38	0.93	16.33	6.36	0.05	3.04	2.12	1.85	3.31	0.17	95.54
7R-1	151.47	61.31	0.95	15.58	7.62	0.07	2.97	1.88	2.06	2.97	0.17	95.57
8R-1	161.50	60.02	0.98	16.89	7.76	0.06	2.89	1.90	2.06	2.91	0.29	95.75
11R-1	190.46	65.28	0.78	13.86	5.29	0.04	2.42	1.63	2.18	2.60	0.16	94.24
12R-2	202.16	60.18	1.00	17.34	7.05	0.05	2.75	1.79	2.03	2.87	0.15	95.20

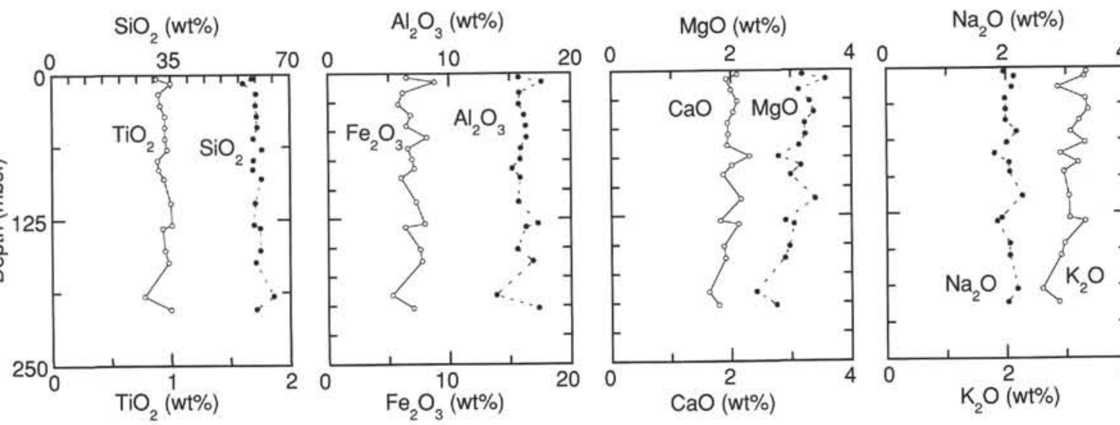

Figure 15. Sediment compositions at Site 912.

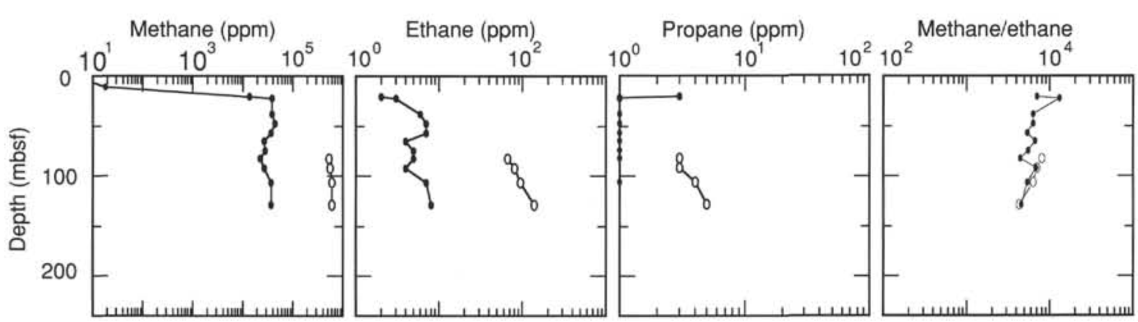

Figure 16. Records of headspace and vacutainer methane (C_1), ethane (C_2), and propane (C_3) concentrations and C_1/C_2 ratios in sediments from Hole 912A. Open circles = vacutainer data, and closed circles = headspace data.

Volatile Hydrocarbons

As part of the shipboard safety and pollution monitoring program, concentrations of methane (C_1), ethane (C_2), and propane (C_3) gases were monitored every core using standard ODP vacutainer and headspace-sampling techniques.

According to the concentrations of headspace methane, the 145.4-m-thick sedimentary section of Hole 912A can be divided into two intervals (Fig. 16, Table 7). The upper about 11.5 mbsf is characterized by very low methane concentrations of 7–18 ppm. Between 11.5 and 23 mbsf, methane concentration distinctly increased from 18 to almost its maximum value of 40,000 ppm. First minor amounts of headspace ethane (2–8 ppm) and propane (1–3 ppm) were determined below about 20 mbsf. The vacutainer concentrations of methane are about 600,000 ppm; ethane and propane vary between 67 and 138 ppm and between 3 and 5 ppm, respectively, increasing downhole (Fig. 16, Table 7).

C_1/C_2 ratios derived from headspace as well as vacutainer analyses are high, ranging from about 4300 to 13,000 ppm, with a decreasing trend downhole (Fig. 16). The high C_1/C_2 ratios suggest in-situ microbial production of methane from marine organic carbon, which is probably present in major quantities (see following section). At

Table 7. Results of headspace and vacutainer gas analysis from Hole 912A.

Core, section, interval top (cm)	Depth (mbsf)	C_1-HS (ppm)	C_2-HS (ppm)	C_3-HS (ppm)	C_1/C_2-HS	C_1-VAC (ppm)	C_2-VAC (ppm)	C_3-VAC (ppm)	C_1/C_2-VAC
151-912A-									
1H-3, 0	3.03	7	0	0					
2H-6, 0	11.53	18	0	0					
3H-6, 0	21.03	13891	2	3	6946				
4H-1, 0	23.03	39225	3	1	13075				
5H-6, 0	40.03	37898	6	1	6316				
6H-6, 0	49.53	44288	7	1	6327				
7H-6, 0	59.03	37571	7	1	5367				
8H-6, 0	68.53	26645	4	1	6661				
9X-6, 0	78.03	27683	5	1	5537				
10X-6, 0	85.53	22473	5	1	4495	538672	67	3	8040
11X-6, 0	95.13	27121	4	0	6780	568207	81	3	7015
13X-4, 0	111.43	37764	7	1	5395	597994	94	4	6362
15X-6, 0	133.63	36602	8	0	4575	597734	138	5	4331

Table 8. Summary of geochemical analyses of sediments in Hole 912A.

Core, section, interval top (cm)	Depth (mbsf)	TC (%)	IC (%)	TOC (%)	$CaCO_3$ (%)	TN (%)	TS (%)	C/N	C/S
151-912A-									
1H-1, 75	0.75	1.28	0.98	0.30	8.2	0.00	0.14		2.1
1H-1, 135	1.35	1.88	0.55	1.33	4.6	0.10	0.22	13.3	6.0
1H-2, 20	1.70	1.16	0.71	0.45	5.9	0.07	0.14	6.4	3.2
1H-2, 53	2.03	0.69	0.45	0.24	3.7	0.06	0.10	4.0	2.4
1H-2, 124	2.74	1.48	0.32	1.16	2.7	0.13	0.17	8.9	6.8
2H-1, 46	4.46	1.50	0.89	0.61	7.4	0.08	0.11	7.6	5.5
2H-3, 102	8.02	0.49	0.23	0.26	1.9	0.05	0.05	5.2	5.2
2H-3, 25	8.55	2.17	0.46	1.71	3.8	0.12	0.27	14.2	6.3
2H-5, 18	10.18	0.74	0.33	0.41	2.7	0.07	0.05	5.8	8.2
2H-5, 92	12.22	1.59	0.40	1.19	3.3	0.11	0.14	10.8	8.5
2H-7, 21	13.21	0.55	0.21	0.34	1.7	0.07	0.00	4.8	
3H-1, 93	14.43	0.57	0.24	0.33	2.0	0.07	0.13	4.7	2.5
3H-3, 18	16.68	1.95	1.38	0.57	11.5	0.08	0.44	7.1	1.3
3H-5, 29	19.79	1.27	0.30	0.97	2.5	0.09	0.40	11.0	2.4
3H-7, 35	22.85	1.28	0.31	0.97	2.6	0.08	0.76	12.0	1.3
4H-1, 106	24.06	1.09	0.28	0.81	2.3	0.10	0.61	8.1	1.3
4H-2, 119	25.69	0.91	0.17	0.74	1.4	0.08	0.85	9.2	0.9
4H-3, 104	27.04	0.91	0.20	0.71	1.7	0.08	0.38	8.9	1.8
4H-4, 94	28.44	0.69	0.22	0.47	1.8	0.08	0.87	5.9	0.5
4H-5, 102	30.02	1.23	0.34	0.89	2.8	0.08	1.08	11.0	0.8
4H-6, 90	31.40	1.28	0.21	1.07	1.7	0.14	0.64	7.6	1.7
4H-7, 34	32.34	1.03	0.21	0.82	1.7	0.10	0.38	8.2	2.1
5H-1, 14	32.64	1.28	0.22	1.06	1.8	0.12	0.38	8.8	2.8
5H-3, 68	36.18	1.35	0.28	1.07	2.3	0.11	0.58	9.7	1.8
5H-5, 70	39.20	1.57	0.42	1.15	3.5	0.11	0.32	10.4	3.6
5H-7, 41	41.91	0.85	0.22	0.63	1.8	0.09	0.31	7.0	2.0
6H-1, 56	42.56	1.44	0.28	1.16	2.3	0.11	0.32	10.5	3.6
6H-3, 130	46.30	1.45	0.21	1.24	1.7	0.13	0.36	9.5	3.4
6H-5, 108	49.08	0.95	0.31	0.64	2.6	0.06	0.41	10.0	1.5
6H-7, 21	51.21	1.28	0.22	1.06	1.8	0.11	0.19	9.6	5.6
7H-1, 99	52.49	1.22	0.29	0.93	2.4	0.11	0.34	8.4	2.7
7H-3, 99	55.49	1.48	0.29	1.19	2.4	0.11	0.33	10.8	3.6
7H-5, 84	58.34	1.44	0.22	1.22	1.8	0.13	0.57	9.4	2.1
7H-7, 49	60.99	1.66	0.21	1.45	1.7	0.12	0.52	12.1	2.8
8H-1, 88	61.88	1.13	0.28	0.85	2.3	0.12	0.11	7.1	7.7
8H-3, 87	64.87	1.40	0.20	1.20	1.7	0.12	0.38	10.0	3.2
8H-5, 70	67.70	1.73	0.28	1.45	2.3	0.14	0.12	10.3	12.1
8H-7, 26	70.26	1.07	0.29	0.78	2.4	0.08	0.10	9.7	7.8
9X-1, 101	71.51	0.77	0.18	0.59	1.5	0.10	0.05	5.9	12.0
9X-3, 112	74.62	1.15	0.22	0.93	1.8	0.12	0.17	7.7	5.5
9X-5, 21	76.71	1.46	0.34	1.12	2.8	0.14	0.14	8.0	8.0
10X-1, 18	78.18	1.26	0.50	0.76	4.2	0.13	0.16	5.8	4.7
10X-3, 19	81.19	1.33	0.62	0.71	5.2	0.12	0.13	5.9	5.4
10X-5, 18	84.18	1.15	0.16	0.99	1.3	0.14	0.19	7.1	5.2
11X-1, 24	87.84	0.87	0.15	0.72	1.2	0.09	0.11	8.0	6.5
11X-2, 24	89.34	1.38	0.26	1.12	2.2	0.13	0.55	8.6	2.0
11X-3, 24	90.84	1.43	0.53	0.90	4.4	0.09	0.15	10.0	6.0
11X-5, 24	93.84	0.91	0.18	0.73	1.5	0.09	0.30	8.1	2.4
11X-7, 24	96.65	1.16	0.29	0.87	2.4	0.09	0.20	9.6	4.3
13X-1, 119	108.09	1.45	0.39	1.06	3.2	0.12	0.12	8.8	8.8
13X-3, 119	111.09	1.04	0.21	0.83	1.7	0.11	0.19	7.5	4.3
13X-5, 119	113.93	1.29	0.29	1.00	2.4	0.11	0.19	9.1	5.3
15X-1, 51	126.61	1.65	0.33	1.32	2.7	0.14	0.20	9.4	6.6
15X-3, 20	128.85	1.49	0.27	1.22	2.2	0.13	0.11	9.4	11.1
15X-5, 20	131.80	1.00	0.26	0.74	2.2	0.11	0.07	6.7	10.0

Notes: IC = inorganic carbon; $CaCO_3$ = carbonate; TC = total carbon; TOC = total organic carbon; TN = total nitrogen, TS = total sulfur; C/N = total organic carbon/total nitrogen ratios; C/S = total organic carbon/total sulfur ratios.

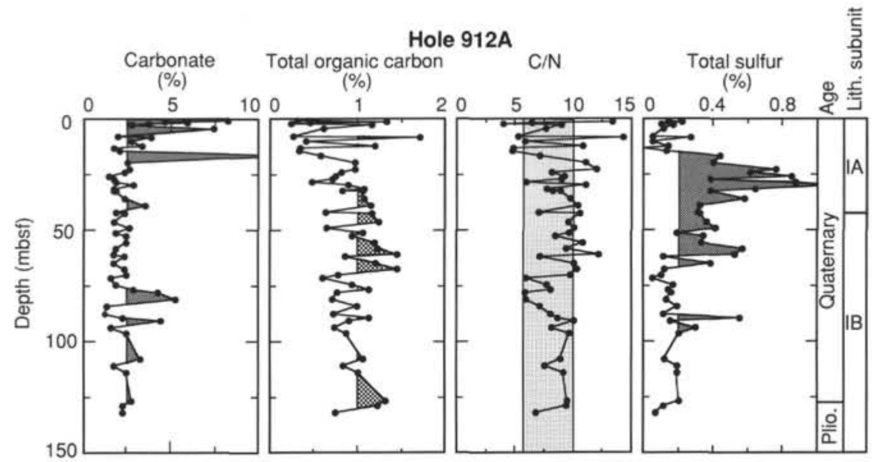

Figure 17. Carbonate contents, total organic carbon contents, organic carbon/total nitrogen (C/N) ratios, and total sulfur contents in sediments from Hole 912A. Shaded area in the C/N record marks range of dominantly marine organic matter; C/N ratios >10 may suggest significant amounts of terrigenous organic matter.

Hole 912A, the methanogenesis has begun at shallow depths around 15 mbsf, as clearly indicated by the sharp increase in methane concentrations and the contemporaneous sharp cessation of sulfate reduction (see "Inorganic Geochemistry" section, this chapter). Unfortunately, the sampling density is not close enough to determine more accurately the depth of the transition between sulfate reduction and methane production.

Carbon, Nitrogen, and Sulfur Concentrations

The results of determinations of inorganic carbon, carbonate, total carbon, total nitrogen, and total sulfur are summarized in Table 8 and presented in Figures 17 and 18.

Most of the carbonate values of the 145.4-m-thick sedimentary sequence of Hole 912A vary between 1.5% and 4%, with the higher values occurring between 77 and 92 mbsf and in the upper 18 m (Fig. 17). Single peaks of carbonate contents as high as 7.4% to 11.5% occur at 0.8, 4.5, and 16.7 mbsf (Fig. 17, Table 8). The origin of the carbonate might be inorganic and/or biogenic, because in the upper part of the hole significant amounts of foraminifers (see "Biostratigraphy" section, this chapter) as well as inorganic carbonate (see "Lithostratigraphy" section, this chapter) exist.

The total organic carbon (TOC) values vary between 0.3% and 1.7% (Fig. 17). In the upper 15 m, both the minimum and maximum values occur, reflecting high-amplitude variations in organic carbon typical for this interval. According to increased C/N ratios, the peak TOC values suggest increased proportions of terrigenous organic matter present in these sediments. Between 15 and 131.8 mbsf, TOC values range from 0.6% to 1.4%, with the lower values more typical in the middle part of this interval. C/N ratios between 6 and 11 point to the presence of significant amounts of marine organic carbon (Figs. 17 and 18; for use of C/N ratios as organic-carbon type indicator see Stein [1991a] and further references therein). Before an interpretation of the organic carbon data in terms of paleoenvironment and its change through time is possible, however, much more data about the composition of the organic matter as well as flux rates are required.

In general, the total sulfur values vary between 0.1% and 1.1% (Fig. 17). Based on this sulfur data, the sedimentary sequences of Hole 912A can be divided into three intervals. Sulfur values of dominantly <0.2% are typical below 90 mbsf and in the upper 15 mbsf. In between these intervals, a distinct sulfur maximum was recorded. The sharp decrease in sulfur at about 15 mbsf coincided with a major drop in magnetic susceptibility, magnetic intensity, and wet-bulk density (see "Paleomagnetics" and "Physical Properties" sections, respectively, this chapter) as well as the transition zone between sulfate reduction and methane production. This change probably reflects a distinct change in mineralogy and redox potential (i.e., a change in the presence of Fe-oxides in the upper 15 m and Fe-sulfides >15 mbsf).

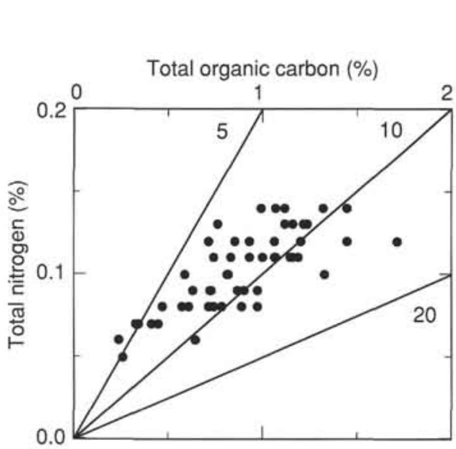

Figure 18. Total organic carbon vs. total nitrogen diagram. Lines of C/N ratios of 5, 10, and 20 are indicated.

PHYSICAL PROPERTIES

Introduction

The shipboard physical properties program at Site 912 included nondestructive measurements of bulk density, bulk magnetic susceptibility, and total natural gamma activity on whole sections of core using the multi-sensor track (MST), as well as discrete measurements of thermal conductivity, compressional-wave velocity, shear strength, and index properties. The downhole temperature measurements are also reported here. Methodology is discussed in the "Explanatory Notes" chapter (this volume).

Whole-core Measurements

Multi-sensor Track

Whole-core magnetic susceptibility, GRAPE density, and natural gamma activity were measured on all of the cores from Holes 912A

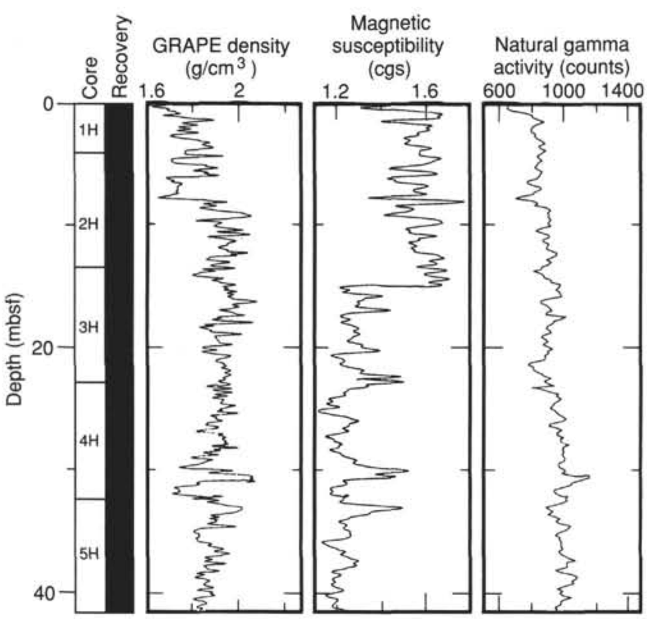

Figure 19. Downhole GRAPE density (g/cm^3), magnetic susceptibility (units are uncorrected cgs Bartington meter units), and total natural gamma activity (units are arbitrary but are based on total gamma counts recorded by a detector) in Hole 912A. All data have been low-pass filtered.

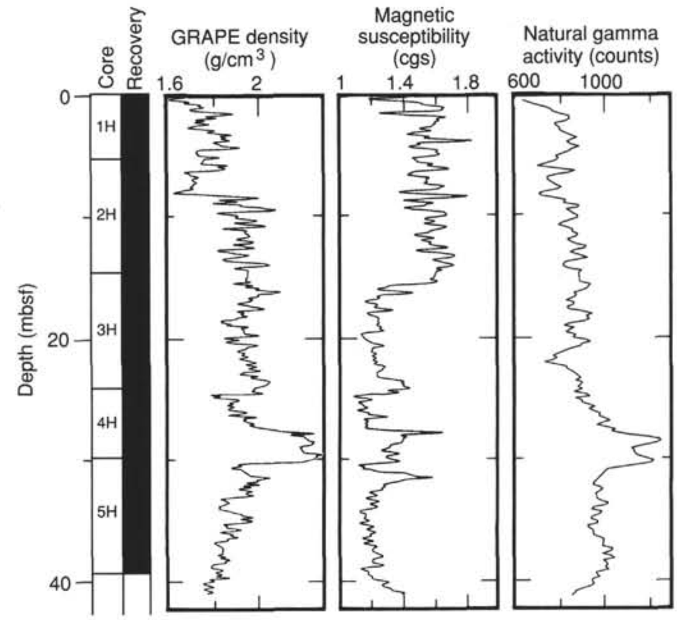

Figure 20. Downhole GRAPE density (g/cm^3), magnetic susceptibility (units are uncorrected cgs Bartington meter units), and total natural gamma activity (units are arbitrary but are based on total gamma counts recorded by a detector) in Hole 912B. All data have been low-pass filtered.

and 912B using the sensors on the multi-sensor track. No MST measurements were performed on the whole cores from Hole 912C because of poor core recovery. The MST data are displayed vs. depth in Figures 19 and 20, for Holes 912A and 912B, respectively. The MST records were low-pass filtered to highlight the gross trends.

A notable feature of the GRAPE density record in Hole 912A is the abrupt increase in bulk density from about 1.65 g/cm^3 to about 2.05 g/cm^3 near 9 mbsf (Fig. 19). Additional abrupt changes in density are observed in the upper 90 mbsf of Hole 912A, where the data coverage is optimum; below 90 mbsf the core recovery limits the data quality. The magnetic susceptibility is initially high, decreases abruptly at about 15 mbsf, fluctuates above an average value of about 1.2 (cgs units) in the interval from 15 to 42 mbsf. The natural gamma activity seems to mimic the general trend of the GRAPE density curve, but exhibits smaller-scale fluctuations relative to the density record.

The MST measurements in Hole 912B (Fig. 20) are quite similar to the data from Hole 912A in the upper 40 mbsf (Fig. 19). GRAPE density increases abruptly at 8 mbsf, and a well-defined density peak between 27 and 30 mbsf corresponds to similar features in Hole 912A. Similarly, both the magnetic susceptibility decrease at 15 mbsf and the double peak near 30 mbsf are observed in the records from each hole; the natural gamma record is likewise comparable between Holes 912A and 912B.

Thermal Conductivity

Thermal conductivities measured at Site 912 are given in Table 9 and are illustrated in Figures 21 and 22, for Holes 912A and 912B, respectively. The conductivity data are plotted along with downhole trends in laboratory values of dry density, void ratio, and shear strength. Thermal conductivity measurements typically were performed at about 75 cm in four whole-round core sections from each core; a black rubber standard (cond. = 0.54 ± 0.02 W/m·K) was used each time to evaluate the degree of error in the measurements. The conductivities measured from the seafloor to 132.4 mbsf range from 1.0 to 1.9 W/m·K. Scatter in the data generally corresponds to changes in water content, the relative abundance of the various sedimentologic components, and to changes in the sand/silt/clay ratio.

Downhole Temperature Measurements and Geothermal Gradient

Downhole temperatures were determined at the seafloor and at two depths in Hole 912A using the Adara Temperature Tool; an additional measurement was performed using the downhole water sampler and temperature probe (WSTP). The temperature at the seafloor was used to intercalibrate the two tools. The equilibrium temperature was calculated as explained in the "Explanatory Notes" chapter (this volume). The results are as follows: Mud line, –0.41°C; 32.5 mbsf, 1.46°C; 61.0 mbsf, 3.23°C; and 97.2 mbsf, 6.88°C. The geothermal gradient determined by a least squares fit of these data was estimated at 64.8°C/km (Fig. 23). This thermal gradient and a range of thermal conductivity values from 1.0 to 1.9 W/m·K were used to estimate the heat flow at Site 912 as between 65 and 123 W/m^2.

Split-core Measurements

Compressional-wave Velocity

Relatively few velocity measurements were performed at Site 912, due to poor quality of the material and its gassy nature. These data are given in Table 10.

Shear Strength

Shear strength measurements were routinely performed in the sediment from split half-cores from Hole 912A and 912B using the mechanical vane throughout, and using a hand-held penetrometer after the sediment attained a certain minimum stiffness. The results of the vane and penetrometer strength measurements are given in Table 11 and are illustrated in Figures 21 and 22. Strength using the vane varied from 5 to 90 kPa in Hole 912A, and up to 250 kPa in Hole 912B. Penetrometer strength measurements reported are the average of two to three measurements at each depth.

Index Properties

Gravimetric determinations of index properties were made for samples in Holes 912A and 912B at the rate of about 2 samples/core section (see Table 12). The representative index properties are shown

Table 9. Thermal conductivity measurements, Site 912.

Core, section, interval top (cm)	Depth (mbsf)	M	P #	TC_{corr} (W/m·K)	Std dev (W/m·K)	Drift (°C/min)
151-912A-						
1H-1, 75	0.75	F	332	1.382	0.00331	0.024
1H-2, 75	2.25	F	338	1.356	0.00436	–0.003
1H-3, 35	3.35	F	339	1.411	0.00256	–0.001
2H-2, 75	6.25	F	332	1.029	0.00321	0.005
2H-3, 75	7.75	F	338	1.423	0.00319	0.018
2H-5, 75	10.75	F	339	1.542	0.00208	0.004
2H-6, 75	12.25	F	350	1.778	0.00243	0.015
3H-2, 75	15.75	F	332	1.323	0.00266	0.025
3H-3, 75	17.25	F	338	1.457	0.00328	0.021
3H-5, 75	20.25	F	339	1.173	0.00963	0.010
3H-6, 75	21.75	F	350	1.432	0.00278	0.014
4H-2, 75	25.25	F	332	1.421	0.00208	0.021
4H-3, 75	26.75	F	338	1.178	0.00263	0.010
4H-6, 75	31.25	F	350	1.132	0.00301	0.037
5H-2, 75	34.75	F	332	1.396	0.00176	0.016
5H-3, 75	36.25	F	338	1.189	0.00242	
5H-4, 75	37.75	F	350	1.628	0.00198	0.027
5H-5, 75	39.25	F	339	1.265	0.00271	0.013
6H-2, 75	44.25	F	332	1.222	0.00200	0.025
6H-3, 75	45.75	F	338	1.165	0.00198	
6H-4, 75	47.25	F	339	1.732	0.00274	0.023
6H-5, 75	48.75	F	350	1.803	0.00200	0.027
7H-2, 75	53.75	F	332	1.101	0.00272	0.023
7H-2, 75	53.75	F	332	1.089	0.00220	0.020
7H-3, 75	55.25	F	338	1.342	0.00372	0.010
7H-4, 75	56.75	F	339	1.508	0.00275	0.024
7H-5, 75	58.25	F	350	1.535	0.00255	0.016
8H-2, 75	63.25	F	350	1.315	0.00155	0.010
8H-3, 75	64.75	F	339	1.014	0.00241	0.011
8H-4, 75	66.25	F	338	1.347	0.00116	0.007
8H-5, 75	67.75	F	332	1.190	0.00209	0.022
9X-2, 75	72.75	F	332	1.439	0.00161	0.013
9X-3, 75	74.25	F	338	1.556	0.00223	0.029
9X-4, 75	75.75	F	339	1.006	0.00599	–0.030
9X-5, 75	77.25	F	350	1.452	0.00229	0.021
9X-5, 75	77.25	F	350	1.467	0.00200	0.024
10X-2, 75	80.25	F	332	1.405	0.00227	0.028
10X-3, 75	81.75	F	338	1.227	0.00290	0.020
10X-4, 75	83.25	F	339	1.441	0.00276	–0.001
10X-5, 75	84.75	F	350	1.484	0.00162	0.026
11X-3, 75	91.35	F	338	1.305	0.00282	0.033
11X-5, 75	94.35	F	339	1.377	0.00353	0.034
11X-6, 75	95.85	F	350	1.668	0.00313	0.039
13X-2, 75	109.15	F	332	1.264	0.00237	0.021
13X-3, 75	110.65	F	338	1.218	0.00362	0.030
13X-4, 75	112.07	F	339	1.412	0.00363	0.011
15X-2, 75	128.27	F	332	1.559	0.00232	0.025
15X-3, 75	129.40	F	338	1.071	0.00324	–0.003
15X-4, 75	130.90	F	339	1.239	0.00315	0.018
15X-5, 75	132.35	F	350	1.342	0.00196	0.003
151-912B-						
1H-1, 75	0.75	F	332	1.189	0.00302	0.020
1H-2, 75	2.25	F	338	1.363	0.00260	0.018
1H-3, 75	3.75	F	339	1.299	0.00266	0.007
1H-4, 28	4.78	F	350	1.378	0.00351	0.021
2H-2, 75	7.55	F	332	1.074	0.00295	0.011
2H-3, 75	9.05	F	338	1.529	0.00418	0.007
2H-5, 75	12.05	F	339	1.664	0.00200	0.035
2H-6, 75	13.55	F	350	1.773	0.00337	–0.003
3H-2, 75	17.05	F	332	1.500	0.00255	0.015
3H-3, 75	18.55	F	338	1.335	0.00303	0.006
3H-5, 75	21.55	F	339	1.575	0.00389	0.035
3H-6, 75	23.05	F	350	1.797	0.00388	0.020
4H-2, 75	26.55	F	332	1.371	0.00201	0.011
4H-3, 75	28.05	F	338	1.446	0.00199	0.010
4H-4, 75	29.55	F	339	1.699	0.00456	0.016
5H-2, 75	33.25	F	332	1.271	0.00227	0.019
5H-3, 75	34.75	F	338	1.456	0.00106	0.002
5H-4, 75	36.25	F	339	1.375	0.00296	0.011
5H-5, 75	37.75	F	350	1.292	0.00200	–0.012

Notes: M = method used, F = full-space or H = half-space; P # = probe number for test; TC_{corr} = thermal conductivity corrected for drift; Std dev = standard deviation of measurement.

in Figures 21 and 24 for Hole 912A (0–145.4 mbsf) and Figures 22 and 25 for Hole 912B (0–40.5 mbsf).

Geotechnical Units

Statistical data abstracted from the index properties determined in the laboratory were used to construct a series of units with respect to geotechnical properties. Three geotechnical units were identified in Hole 912A: an upper zone of highly variable but generally low bulk densities and high porosities, consisting of silty clay without dropstones from the seafloor to ~8 mbsf (geotechnical Unit G-I); a zone of silty clay to silty mud having variable amounts of dropstones between 8 and about 50 mbsf, with increased but highly variable bulk density values and inversely related trends in water content and porosity (geotechnical Unit G-II); and a zone below about 50 mbsf where the physical properties seem to become more constant and the core recovery is reduced (geotechnical Unit G-III).

Ms 151IR-110

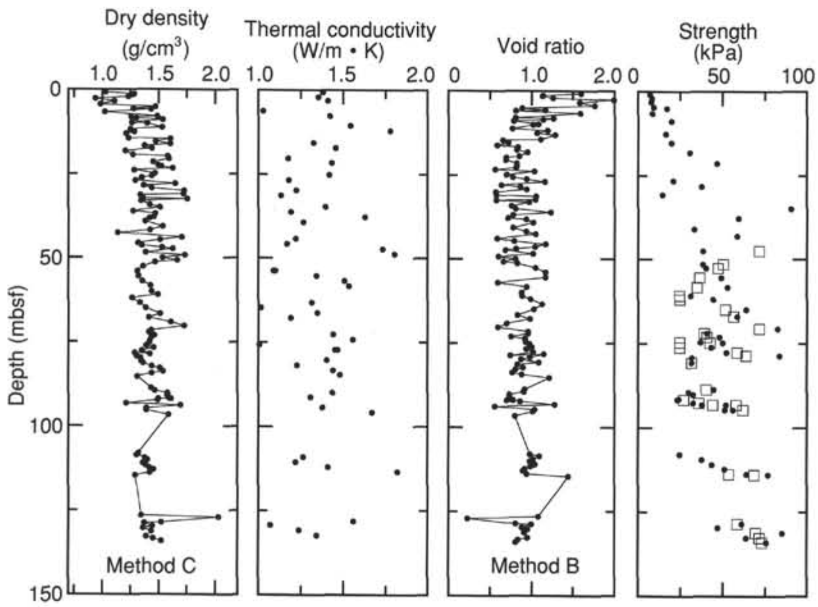

Figure 21. Comparison of laboratory index property measurements, thermal conductivity, and peak shear strength vs. depth in Hole 912A. Shear strength was measured using the mechanical vane (closed circles) and using the hand-held penetrometer (open squares).

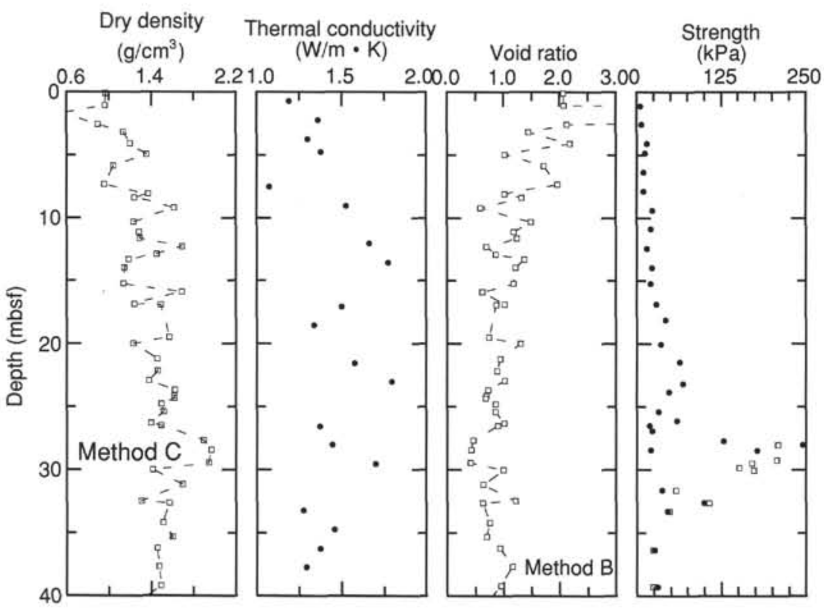

Figure 22. Comparison of laboratory index property measurements, thermal conductivity, and peak shear strength vs. depth in Hole 912B. Shear strength was measured using the mechanical vane (closed circles) and using the hand-held penetrometer (open squares).

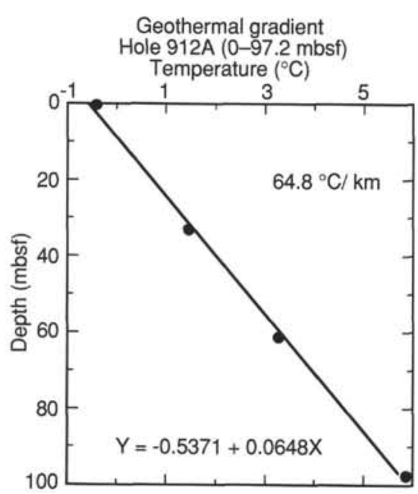

Figure 23. Downhole temperature measurements in Hole 912A.

Table 10. Compressional-wave velocity measurements, Site 912.

Core, section, interval (cm)	Depth (mbsf)	Tool	Velocity (m/s) Perp	Par
151-912A-				
1H-1, 100–107	1.00	dsv	1565	
1H-2, 50–57	2.00	dsv	1543	
1H-3, 24–31	3.24	dsv	1599	
2H-3, 45–52	7.45	dsv	1556	
3H-2, 42–49	15.42	dsv	1599	
151-912B-				
1H-1, 50–57	0.50	dsv	1558	
1H-2, 50–57	2.00	dsv	1567	
1H-3, 43–50	3.43	dsv	1510	
2H-1, 50–57	5.80	dsv	1560	
2H-2, 50–57	7.30	dsv	1539	
2H-3, 50–57	8.80	dsv	1568	
2H-5, 50–57	11.80	dsv	1484	
2H-6, 50–57	13.30	dsv	1626	
3H-1, 40–47	15.20	dsv	1615	
3H-2, 53–60	16.83	dsv	1592	
3H-3, 32–39	18.12	dsv	1586	

Note: Tool = device used for measurement, either dsv = digital sound velocimeter or ham = Hamilton Frame. Perp = perpendicular, Par = parallel.

Table 11. Shear strength measurements, Site 912.

Core, section interval (cm)	Depth (mbsf)	SN	Vane (kPa)	Res (kPa)	Pen (kPa)
151-912A-					
1H-1, 105–106	1.05	1	7	4	
1H-2, 55–56	2.05	1	8	4	
1H-3, 28–29	3.28	1	8	5	
2H-1, 84–85	4.84	1	9	6	
2H-1, 122–123	5.22	1	17	10	
2H-2, 115–116	6.65	1	9	2	
2H-4, 45–46	8.95	1	20	10	
2H-6, 119–120	12.69	1	16	8	
3H-2, 45–46	15.45	1	20	9	
3H-4, 33–34	18.33	1	31	16	
3H-6, 53–54	21.53	1	47	20	
4H-3, 65–66	26.65	1	21	9	
4H-4, 92–93	28.42	1	38	20	
4H-6, 35–36	30.85	1	15	7	
5H-2, 103–104	35.03	1	91	60	
5H-6, 110–111	41.10	1	33	14	
6H-1, 110–111	43.10	1	59	19	
6H-4, 95–96	47.45	1	39	18	72
6H-7, 47–48	51.47	1	39	15	51
7H-1, 100–101	52.50	1	40	14	47
7H-3, 100–101	55.50	1	49	18	37
7H-5, 86–87	58.36	1	53		36
7H-7, 25–26	60.75	1	31	13	26
8H-1, 85–86	61.85	1	45	16	26
8H-3, 85–86	64.85	1	64	58	51
8H-5, 10–11	67.10	1	59	18	66
8H-7, 65–66	70.65	1	83	27	72
9H-1, 136–137	71.86	3	41	19	39
9H-2, 110–111	73.10	3	48	18	41
9H-3, 111–112	74.70	3	50	23	42
9H-3, 120–121	74.61	3	37	20	25
9H-4, 110–111	76.10	3	43	18	26
9H-5, 118–119	77.68	3	53	17	69
9H-6, 50–51	78.50	3	84		64
10H-1, 110–111	79.10	3	32	15	
10H-2, 110–111	80.60	3	32	14	32
11H-3, 110–111	88.70	3	45	19	40
11H-4, 110–111	90.20	3	32	14	
11H-5, 110–111	89.35	3	30	14	
11H-1, 110–111	91.70	3	23	12	27
11H-2, 25–26	91.52	3	24	12	
11H-2, 110–111	93.20	3	38	19	44
11H-3, 92–93	93.20	3	52	27	
11H-4, 45–46	92.55	3	33	15	36
11H-4, 110–111	94.70	3	56	15	62
11H-5, 110–111	94.70	3	51	23	
13H-1, 110–111	108.00	3	25	13	
13H-2, 110–111	109.50	3	38	14	
13H-3, 110–111	111.00	3	44	20	
13H-4, 110–111	112.42	3	51	23	
13H-5, 110–111	113.99	3	77	25	69
13H-5, 125–126	113.84	3	64	25	54
15H-2, 100–101	128.52	3	61	25	59
15H-3, 111–112	129.76	3	47	20	
15H-4, 110–111	131.25	3	85	24	69
15H-5, 110–111	132.70	3	64	21	72
15H-6, 110–111	134.20	3	76	23	74
151-912B-					
1H-1, 110–111	1.10	1	6	5	
1H-2, 110–111	2.60	1	7	7	
1H-3, 110–111	4.10	1	15	7	
1H-4, 40–41	4.90	1	12	6	
2H-1, 112–113	6.42	1	11	6	
2H-2, 110–111	7.90	1	10	5	
2H-3, 110–111	9.40	1	23	12	
2H-4, 110–111	10.90	1	21	10	
2H-5, 116–117	12.46	1	15	6	
2H-6, 118–119	13.98	1	22	12	
3H-1, 43–44	15.23	1	20	10	
3H-2, 55–56	16.85	1	29	8	
3H-3, 35–36	18.15	1	42	23	
3H-4, 76–78	20.06	1	36	19	
3H-5, 66–67	21.46	1	63	27	
3H-6, 90–91	23.20	1	680	30	
3H-7, 6–7	23.86	1	48	20	
4H-1, 111–112	25.41	1	31	9	
4H-2, 30–31	26.10	1	18	10	
4H-2, 74–75	26.54	1	59	40	
4H-2, 109–110	26.89	1	22	6	
4H-3, 40–41	27.70				
4H-3, 76–83	28.06	3	178	80	101
4H-3, 113–114	28.43	4	129	60	
4H-3, 120–121	28.50				
4H-4, 44–45	29.24				101
4H-4, 69–70	29.49	4	245	100	83
4H-4, 102–103	29.82				74
4H-4, 125–126	30.05	1	21	9	84
5H-1, 61–62	31.61	1	37	15	28
5H-2, 12–13	32.62	1	99	67	52
5H-2, 78–79	33.28	1	44	19	23
5H-4, 85–86	36.35	1	26	13	12
5H-6, 82–83	39.32	1	31	17	12

Note: SN = numbered spring used to make the measurement. Vane = undrained shear strength; Res = residual shear strength; Pen = unconfined shear strength as measured by the penetrometer. To obtain more accurate penetrometer values, multiply Pen value by 0.98067 (see "Physical Properties" section in the "Explanatory Notes" chapter, this volume).

NOTE: For all sites drilled, core-description forms ("barrel sheets") and core photographs can be found in Section 6, beginning on page 465. Forms containing smear-slide data can be found in Section 7, beginning on page 849. Thin-section descriptions are given in Section 8, beginning on page 885, and sediment thin sections in Section 9, beginning on page 895. Dropstone descriptions are included in Section 10, beginning on page 903.

Table 12. Index property measurements, Site 912.

Core, section, interval (cm)	Depth (mbsf)	WC-d (%)	WC-w (%)	WBD[a] (g/cm^3)	WBD[b] (g/cm^3)	GD[a] (g/cm^3)	GD[b] (g/cm^3)	DBD[a] (g/cm^3)	DBD[b] (g/cm^3)	Por[a] (%)	Por[b] (%)	VR[a]	VR[b]
151-912A-													
1H-1, 77–79	0.77	63.33	38.77	1.63	1.68	2.59	2.83	1.00	1.03	61.54	63.62	1.60	1.75
1H-1, 132–134	1.32	42.37	29.76	1.84	1.82	2.76	2.72	1.29	1.28	53.29	52.93	1.14	1.12
1H-2, 18–20	1.68	43.09	30.11	1.81	1.81	2.69	2.69	1.26	1.26	53.11	53.11	1.13	1.13
1H-2, 54–56	2.04	46.85	31.90	1.79	1.81	2.76	2.81	1.22	1.23	55.77	56.20	1.26	1.28
1H-2, 122–124	2.72	72.23	41.94	1.63	1.62	2.82	2.77	0.94	0.94	66.56	66.12	1.99	1.95
1H-3, 39–41	3.39	55.98	35.89	1.75	1.73	2.90	2.83	1.12	1.11	61.28	60.69	1.58	1.54
2H-1, 47–49	4.47	66.92	40.09	1.63	1.64	2.71	2.76	0.98	0.99	63.87	64.34	1.77	1.80
2H-1, 122–124	5.22	32.16	24.33	1.98	1.95	2.82	2.74	1.50	1.47	46.97	46.19	0.89	0.86
2H-2, 14–16	5.64	43.39	30.26	1.83	1.83	2.77	2.77	1.27	1.28	53.94	53.99	1.17	1.17
2H-2, 37–39	5.87	33.44	25.06	1.83	1.92	2.49	2.70	1.38	1.44	44.86	46.86	0.81	0.88
2H-2, 114–116	6.64	64.36	39.16	1.61	1.68	2.53	2.86	0.98	1.02	61.34	64.21	1.59	1.79
2H-3, 104–106	8.04	30.60	23.43	1.95	1.95	2.69	2.69	1.49	1.49	44.54	44.53	0.80	0.80
2H-3, 123–125	8.23	44.69	30.89	1.85	1.81	2.90	2.76	1.28	1.25	55.85	54.63	1.27	1.20
2H-4, 15–17	8.65	42.16	29.66	1.84	1.85	2.77	2.80	1.29	1.30	53.25	53.50	1.14	1.15
2H-4, 45–47	8.95	28.64	22.26	2.02	1.97	2.80	2.69	1.57	1.54	43.93	42.90	0.78	0.75
2H-4, 142–144	9.92	43.88	30.50	1.74	1.81	2.51	2.74	1.21	1.26	51.82	53.96	1.08	1.17
2H-5, 20–22	10.20	36.14	26.55	1.95	1.90	2.88	2.75	1.43	1.40	50.41	49.23	1.02	0.97
2H-5, 127–129	11.27	28.54	22.20	2.00	1.96	2.74	2.66	1.55	1.53	43.28	42.55	0.76	0.74
2H-6, 26–28	11.76	45.59	31.31	1.78	1.82	2.67	2.81	1.22	1.25	54.32	55.53	1.19	1.25
2H-6, 118–120	12.68	41.75	29.45	1.80	1.82	2.62	2.68	1.27	1.28	51.60	52.21	1.07	1.09
2H-7, 22–24	13.22	46.52	31.75	1.81	1.78	2.83	2.69	1.24	1.21	56.20	55.00	1.28	1.22
3H-1, 94–96	14.44	44.89	30.98	1.74	1.79	2.53	2.69	1.20	1.24	52.57	54.09	1.11	1.18
3H-1, 125–127	14.75	25.71	20.45	1.98	2.02	2.60	2.69	1.57	1.61	39.51	40.26	0.65	0.67
3H-2, 45–47	15.45	30.01	23.08	1.87	1.91	2.47	2.59	1.43	1.47	42.01	43.12	0.72	0.76
3H-2, 125–127	16.25	25.20	20.13	1.88	2.01	2.37	2.65	1.50	1.60	36.83	39.41	0.58	0.65
3H-3, 18–20	16.68	35.46	26.18	1.78	1.86	2.42	2.63	1.32	1.38	45.53	47.59	0.84	0.91
3H-3, 106–108	17.56	33.06	24.85	1.86	1.92	2.54	2.70	1.40	1.44	45.08	46.55	0.82	0.87
3H-4, 34–36	18.34	44.66	30.87	1.62	1.74	2.18	2.54	1.12	1.21	48.72	52.54	0.95	1.11
3H-4, 143–145	19.43	41.39	29.27	1.61	1.79	2.11	2.60	1.14	1.27	45.95	51.26	0.85	1.05
3H-5, 28–30	19.78	25.92	20.58	2.04	1.99	2.74	2.63	1.62	1.58	40.96	39.91	0.69	0.66
3H-5, 100–102	20.50	26.02	20.65	2.03	2.00	2.72	2.66	1.61	1.59	40.86	40.34	0.69	0.68
3H-6, 53–55	21.53	31.21	23.78	1.94	1.91	2.70	2.61	1.48	1.45	45.08	44.29	0.82	0.80
3H-6, 136–138	22.36	30.53	23.39	1.97	1.95	2.75	2.69	1.51	1.49	45.06	44.50	0.82	0.80
3H-7, 35–37	22.85	29.53	22.80	2.02	1.97	2.82	2.72	1.56	1.52	44.86	43.91	0.81	0.78
4H-1, 33–35	23.33	21.07	17.40	2.12	1.97	2.74	2.44	1.75	1.63	36.02	33.44	0.56	0.50
4H-1, 105–107	24.05	42.13	29.64	1.76	1.82	2.51	2.71	1.24	1.28	50.76	52.65	1.03	1.11
4H-2, 41–43	24.91	30.84	23.57	1.79	1.92	2.32	2.64	1.37	1.47	41.16	44.26	0.70	0.79
4H-2, 118–120	25.68	33.28	24.97	1.79	1.92	2.39	2.70	1.34	1.44	43.65	46.72	0.77	0.88
4H-3, 23–25	26.23	37.93	27.50	1.81	1.86	2.55	2.69	1.31	1.35	48.53	49.90	0.94	1.00
4H-3, 104–106	27.04	37.71	27.38	2.01	1.78	3.16	2.46	1.46	1.29	53.74	47.53	1.16	0.91
4H-4, 36–38	27.86	23.91	19.29	2.07	2.04	2.75	2.68	1.67	1.65	39.05	38.45	0.64	0.62
4H-4, 96–98	28.46	37.11	27.07	1.76	1.87	2.40	2.70	1.28	1.37	46.44	49.44	0.87	0.98
4H-5, 17–19	29.17	33.93	25.33	1.96	1.93	2.84	2.75	1.46	1.44	48.48	47.64	0.94	0.91
4H-5, 103–105	30.03	21.04	17.38	2.14	2.09	2.78	2.67	1.77	1.73	36.34	35.44	0.57	0.55
4H-6, 52–54	31.02	21.46	17.67	2.12	2.09	2.75	2.69	1.74	1.72	36.50	36.00	0.57	0.56
4H-6, 90–92	31.40	38.71	27.91	1.89	1.86	2.79	2.71	1.36	1.34	51.34	50.59	1.06	1.02
4H-7, 35–37	32.35	38.03	27.55	1.91	1.88	2.83	2.74	1.38	1.36	51.22	50.44	1.05	1.02
5H-1, 9–11	32.59	20.98	17.34	2.17	2.12	2.83	2.73	1.79	1.75	36.72	35.86	0.58	0.56
5H-1, 60–62	33.10	38.47	27.78	1.81	1.86	2.58	2.71	1.31	1.34	49.20	50.43	0.97	1.02
5H-2, 15–17	34.15	34.15	25.46	1.73	1.91	2.27	2.70	1.29	1.42	43.04	47.40	0.76	0.90
5H-2, 102–104	35.02	29.27	22.64	2.02	1.95	2.82	2.66	1.56	1.51	44.60	43.18	0.81	0.76
5H-3, 65–67	36.15	43.93	30.52	1.86	1.83	2.88	2.80	1.29	1.27	55.27	54.55	1.24	1.20
5H-3, 136–138	36.86	32.10	24.30	1.84	1.94	2.46	2.72	1.39	1.47	43.56	45.97	0.77	0.85
5H-4, 74–76	37.74	32.57	24.57	1.74	1.93	2.25	2.72	1.31	1.46	41.68	46.36	0.71	0.86
5H-4, 114–116	38.14	34.25	25.51	1.94	1.90	2.80	2.69	1.45	1.42	48.31	47.34	0.93	0.90
5H-5, 67–69	39.17	36.70	26.85	1.93	1.88	2.85	2.72	1.41	1.38	50.55	49.35	1.02	0.97
5H-6, 58–60	40.58	28.79	22.36	2.00	1.98	2.75	2.71	1.55	1.54	43.61	43.20	0.77	0.76
5H-7, 38–40	41.88	34.03	25.39	1.95	1.91	2.82	2.69	1.46	1.42	48.35	47.19	0.94	0.89
6H-1, 53–55	42.53	48.24	32.54	1.61	1.69	2.23	2.45	1.09	1.14	51.20	53.55	1.05	1.15
6H-2, 30–32	43.80	21.47	17.67	2.13	2.07	2.77	2.64	1.75	1.70	36.73	35.65	0.58	0.55
6H-2, 117–119	44.67	29.29	22.66	1.99	1.96	2.75	2.67	1.54	1.51	44.04	43.24	0.79	0.76
6H-3, 55–57	45.55	41.31	29.23	1.89	1.86	2.90	2.81	1.34	1.32	53.93	53.07	1.17	1.13
6H-3, 129–131	46.29	37.83	27.45	1.91	1.86	2.83	2.69	1.38	1.35	51.08	49.79	1.04	0.99
6H-4, 43–45	46.93	29.81	22.96	2.00	1.98	2.80	2.75	1.54	1.53	44.88	44.43	0.81	0.80
6H-4, 81–83	47.31	25.05	20.03	2.08	2.03	2.80	2.70	1.66	1.63	40.60	39.75	0.68	0.66
6H-5, 37–39	48.37	36.43	26.70	1.93	1.89	2.85	2.73	1.42	1.38	50.35	49.21	1.01	0.97
6H-5, 107–109	49.07	21.85	17.93	2.15	2.11	2.82	2.74	1.76	1.73	37.57	36.89	0.60	0.58
6H-6, 50–52	50.00	28.88	22.41	2.04	1.98	2.86	2.71	1.59	1.54	44.66	43.31	0.81	0.76
6H-6, 116–118	50.66	24.08	19.40	2.10	2.07	2.81	2.74	1.69	1.67	39.78	39.12	0.66	0.64
6H-7, 25–27	51.25	32.20	24.35	1.91	1.94	2.64	2.73	1.44	1.47	45.30	46.13	0.83	0.86
7H-1, 101–103	52.51	37.70	27.38	1.92	1.88	2.86	2.74	1.39	1.36	51.24	50.15	1.05	1.01
7H-2, 101–103	54.01	41.07	29.12	1.90	1.85	2.93	2.76	1.35	1.31	54.01	52.54	1.17	1.11
7H-3, 101–103	55.51	38.86	27.99	1.98	1.84	3.09	2.66	1.42	1.32	53.99	50.21	1.17	1.01
7H-4, 101–103	57.01	37.32	27.18	1.41	1.86	1.64	2.67	1.03	1.35	37.33	49.28	0.60	0.97
7H-5, 85–87	58.35	33.91	25.32	1.96	1.92	2.84	2.72	1.46	1.43	48.45	47.36	0.94	0.90
7H-6, 101–103	60.01	32.54	24.55	1.96	1.91	2.79	2.65	1.48	1.44	46.93	45.67	0.88	0.84
7H-7, 51–53	61.01	31.07	23.71	2.03	1.96	2.92	2.73	1.55	1.50	46.97	45.32	0.89	0.83
8H-1, 86–88	61.86	43.65	30.39	1.68	1.82	2.32	2.74	1.17	1.27	49.66	53.89	0.99	1.17
8H-2, 86–88	63.36	39.59	28.36	1.92	1.86	2.92	2.74	1.37	1.33	53.00	51.42	1.13	1.06
8H-3, 86–88	64.86	36.20	26.58	1.95	1.89	2.90	2.71	1.43	1.38	50.56	48.90	1.02	0.96
8H-4, 107–109	66.57	29.52	22.79	2.03	1.96	2.86	2.69	1.57	1.51	45.19	43.62	0.82	0.77
8H-5, 68–70	67.68	34.84	25.84	1.97	1.90	2.89	2.71	1.46	1.41	49.55	47.95	0.98	0.92
8H-6, 69–71	69.19	25.79	20.50	2.06	2.03	2.78	2.71	1.64	1.61	41.15	40.51	0.70	0.68
8H-7, 23–25	70.23	21.36	17.60	2.17	2.09	2.85	2.69	1.79	1.73	37.25	35.95	0.59	0.56
9X-1, 100–102	71.50	34.27	25.52	1.96	1.93	2.86	2.76	1.46	1.43	48.86	47.96	0.96	0.92
9X-2, 20–22	72.20	34.72	25.77	1.94	1.91	2.82	2.72	1.44	1.41	48.86	47.91	0.96	0.92
9X-2, 110–112	73.10	33.07	24.85	1.77	1.95	2.32	2.77	1.33	1.46	42.82	47.22	0.75	0.89
9X-3, 20–22	73.70	33.48	25.08	1.96	1.92	2.81	2.70	1.47	1.44	47.88	46.90	0.92	0.88

Table 12 (continued).

Core, section, interval (cm)	Depth (mbsf)	WC-d (%)	WC-w (%)	WBD[a] (g/cm³)	WBD[b] (g/cm³)	GD[a] (g/cm³)	GD[b] (g/cm³)	DBD[a] (g/cm³)	DBD[b] (g/cm³)	Por[a] (%)	Por[b] (%)	VR[a]	VR[b]
9X-3, 110–112	74.60	33.79	25.26	1.95	1.90	2.80	2.67	1.46	1.42	48.01	46.85	0.92	0.88
9X-4, 20–22	75.20	35.02	25.94	1.95	1.91	2.85	2.75	1.44	1.42	49.34	48.45	0.97	0.94
9X-4, 110–112	76.10	36.16	26.56	1.93	1.89	2.83	2.73	1.42	1.39	49.96	49.06	1.00	0.96
9X-5, 20–22	76.70	33.48	25.08	1.97	1.94	2.86	2.78	1.48	1.46	48.29	47.56	0.93	0.91
9X-5, 116–118	77.66	37.33	27.18	1.90	1.86	2.79	2.66	1.38	1.35	50.38	49.24	1.02	0.97
9X-6, 59–61	78.59	33.73	25.22	1.73	1.90	2.25	2.67	1.29	1.42	42.59	46.81	0.74	0.88
10X-1, 20–22	78.20	41.66	29.41	1.86	1.83	2.82	2.71	1.31	1.29	53.38	52.38	1.14	1.10
10X-1, 110–112	79.10	40.43	28.79	1.76	1.83	2.49	2.68	1.26	1.30	49.55	51.40	0.98	1.06
10X-2, 20–22	79.70	38.42	27.76	1.72	1.85	2.32	2.69	1.24	1.34	46.50	50.22	0.87	1.01
10X-2, 110–112	80.60	38.27	27.68	1.93	1.86	2.91	2.71	1.39	1.35	52.07	50.26	1.09	1.01
10X-3, 20–22	81.20	36.97	26.99	1.72	1.87	2.30	2.68	1.26	1.36	45.35	49.19	0.83	0.97
10X-3, 110–112	82.10	32.94	24.78	1.96	1.91	2.80	2.67	1.47	1.44	47.36	46.23	0.90	0.86
10X-4, 20–22	82.70	29.56	22.82	2.00	1.96	2.79	2.68	1.55	1.51	44.58	43.58	0.80	0.77
10X-4, 110–112	83.60	28.23	22.02	2.02	1.98	2.79	2.68	1.58	1.54	43.43	42.44	0.77	0.74
10X-5, 20–22	84.20	33.09	24.86	1.93	1.92	2.72	2.70	1.45	1.44	46.76	46.58	0.88	0.87
10X-5, 110–112	85.10	40.54	28.85	1.95	1.84	3.08	2.72	1.39	1.31	54.92	51.86	1.22	1.08
11X-1, 110–112	88.70	33.71	25.21	1.95	1.92	2.79	2.72	1.45	1.43	47.84	47.19	0.92	0.89
11X-2, 20–22	89.30	32.50	24.53	1.98	1.94	2.85	2.74	1.50	1.47	47.48	46.46	0.90	0.87
11X-2, 110–112	90.20	26.96	21.23	2.04	2.01	2.78	2.71	1.60	1.58	42.19	41.62	0.73	0.71
11X-3, 20–22	90.80	26.82	21.15	2.04	1.99	2.78	2.67	1.61	1.57	42.07	41.15	0.73	0.70
11X-3, 104–106	91.64	26.89	21.19	2.07	2.02	2.85	2.73	1.63	1.59	42.74	41.70	0.75	0.72
11X-3, 118–120	91.78	25.97	20.62	2.04	2.03	2.75	2.72	1.62	1.61	41.07	40.79	0.70	0.69
11X-3, 124–126	91.84	30.17	23.18	1.93	1.95	2.63	2.68	1.48	1.50	43.67	44.07	0.78	0.79
11X-4, 20–22	92.30	31.07	23.71	2.00	1.95	2.83	2.71	1.52	1.49	46.21	45.13	0.86	0.82
11X-4, 110–112	93.20	46.67	31.82	1.81	1.77	2.80	2.69	1.23	1.21	56.06	55.04	1.28	1.22
11X-5, 20–22	93.80	21.92	17.98	2.03	2.06	2.58	2.65	1.66	1.69	35.53	36.18	0.55	0.57
11X-5, 110–112	94.70	36.33	26.65	1.95	1.90	2.91	2.74	1.43	1.39	50.78	49.28	1.03	0.97
11X-6, 20–22	95.30	36.35	26.66	1.93	1.90	2.84	2.74	1.42	1.39	50.21	49.30	1.01	0.97
11X-7, 20–22	96.61	26.99	21.25	2.14	2.01	3.04	2.72	1.69	1.58	44.45	41.72	0.80	0.72
13X-1, 110–112	108.00	39.00	28.06	1.81	1.84	2.57	2.66	1.30	1.32	49.46	50.27	0.98	1.01
13X-2, 20–22	108.60	40.10	28.62	1.87	1.83	2.80	2.66	1.34	1.30	52.28	50.99	1.10	1.04
13X-2, 110–112	109.50	36.99	27.00	1.92	1.89	2.83	2.74	1.40	1.38	50.49	49.73	1.02	0.99
13X-3, 20–22	110.10	35.50	26.20	1.93	1.90	2.83	2.72	1.43	1.40	49.46	48.55	0.98	0.94
13X-3, 113–115	111.03	37.47	27.26	1.91	1.87	2.84	2.71	1.39	1.36	50.92	49.81	1.04	0.99
13X-4, 20–22	111.52	35.63	26.27	1.94	1.87	2.84	2.66	1.43	1.38	49.65	48.05	0.99	0.92
13X-4, 110–112	112.42	33.78	25.25	1.94	1.90	2.78	2.66	1.45	1.42	47.86	46.72	0.92	0.88
13X-5, 20–22	112.94	32.83	24.71	1.96	1.93	2.80	2.73	1.48	1.46	47.29	46.63	0.90	0.87
13X-5, 110–112	113.84	34.31	25.55	1.95	1.91	2.82	2.71	1.45	1.42	48.57	47.54	0.94	0.91
15X-1, 50–52	126.60	37.43	27.24	1.95	1.85	2.94	2.64	1.42	1.34	51.81	49.07	1.08	0.96
15X-2, 100–102	128.52	29.52	22.79	2.01	1.97	2.80	2.72	1.55	1.52	44.67	43.91	0.81	0.78
15X-3, 20–22	128.85	36.51	26.74	1.91	1.88	2.80	2.69	1.40	1.37	49.94	48.95	1.00	0.96
15X-3, 110–112	129.75	32.81	24.71	1.95	1.92	2.76	2.69	1.47	1.44	46.92	46.24	0.88	0.86
15X-4, 24–26	130.39	36.21	26.58	1.88	1.85	2.68	2.62	1.38	1.36	48.64	48.10	0.95	0.93
15X-4, 108–110	131.23	32.98	24.80	1.97	1.91	2.82	2.67	1.48	1.44	47.57	46.18	0.91	0.86
15H-5, 20–22		29.51	22.79	2.00	1.97	2.77	2.71	1.54	1.52	44.39	43.80	0.80	0.78
15X-5, 110–112	132.70	35.82	26.37	1.89	1.89	2.72	2.71	1.39	1.39	48.71	48.62	0.95	0.95
15X-6, 20–22	133.30	31.62	24.03	1.94	1.91	2.70	2.63	1.47	1.45	45.44	44.84	0.83	0.81
15X-6, 110–112	134.20	29.12	22.55	2.02	1.97	2.82	2.70	1.57	1.53	44.49	43.36	0.80	0.77
151-912B-													
1H-1, 10–12	0.10	69.73	41.08	1.68	1.65	3.04	2.86	0.99	0.97	67.39	66.02	2.07	1.94
1H-1, 108–110	1.08	69.36	40.96	1.69	1.63	3.07	2.76	1.00	0.96	67.48	65.17	2.07	1.87
1H-2, 108–110	2.58	76.87	43.46	1.61	1.59	2.85	2.77	0.91	0.90	68.14	67.54	2.14	2.08
1H-3, 20–22	3.20	51.81	34.13	1.78	1.73	2.87	2.68	1.17	1.14	59.20	57.52	1.45	1.35
1H-3, 110–112	4.10	47.86	32.37	2.17	1.77	4.67	2.71	1.47	1.20	68.58	55.87	2.18	1.27
1H-4, 45–47	4.95	37.65	27.35	1.90	1.86	2.79	2.68	1.38	1.35	50.59	49.61	1.02	0.98
2H-1, 58–60	5.88	60.69	37.77	1.71	1.68	2.89	2.74	1.07	1.04	63.15	61.85	1.71	1.62
2H-2, 53–55	7.33	68.99	40.83	1.66	1.62	2.92	2.70	0.99	0.96	66.31	64.50	1.97	1.82
2H-2, 131–133	8.11	36.89	26.95	1.92	1.87	2.83	2.69	1.40	1.37	50.43	49.23	1.02	0.97
2H-3, 12–14	8.42	45.39	31.22	1.87	1.80	2.98	2.75	1.29	1.24	56.91	54.93	1.32	1.22
2H-3, 92–94	9.22	25.31	20.20	1.88	2.02	2.38	2.68	1.50	1.61	37.04	39.86	0.59	0.66
2H-4, 51–53	10.31	47.10	32.02	1.92	1.82	3.24	2.86	1.30	1.24	59.85	56.77	1.49	1.31
2H-4, 136–138	11.16	41.75	29.45	1.88	1.81	2.88	2.67	1.33	1.28	54.00	52.10	1.17	1.09
2H-5, 36–38	11.66	43.04	30.09	1.88	1.84	2.94	2.81	1.32	1.29	55.24	54.13	1.23	1.18
2H-5, 103–105	12.33	23.19	18.82	2.22	2.08	3.05	2.73	1.80	1.69	40.81	38.17	0.69	0.62
2H-6, 10–12	12.90	33.85	25.29	1.88	1.94	2.61	2.78	1.40	1.45	46.32	47.90	0.86	0.92
2H-6, 51–53	13.31	48.48	32.65	1.81	1.76	2.88	2.70	1.22	1.19	57.68	56.07	1.36	1.28
2H-6, 117–119	13.97	51.61	34.04	1.65	1.73	2.41	2.69	1.09	1.14	54.79	57.52	1.21	1.35
3H-1, 44–46	15.24	52.14	34.27	1.61	1.73	2.30	2.71	1.06	1.14	53.96	57.99	1.17	1.38
3H-1, 108–110	15.88	23.10	18.77	2.12	2.08	2.80	2.73	1.72	1.69	38.73	38.10	0.63	0.62
3H-2, 57–59	16.87	45.07	31.07	1.67	1.80	2.33	2.74	1.15	1.24	50.57	54.63	1.02	1.20
3H-2, 63–65	16.93	31.06	23.70	2.01	1.95	2.87	2.72	1.53	1.49	46.50	45.19	0.87	0.82
3H-4, 19–21	19.49	27.00	21.26	2.05	2.00	2.82	2.69	1.62	1.57	42.62	41.43	0.74	0.71
3H-4, 70–72	20.00	45.57	31.30	1.85	1.79	2.94	2.71	1.27	1.23	56.62	54.64	1.30	1.20
3H-5, 40–42	21.20	33.14	24.89	1.99	1.94	2.90	2.76	1.50	1.46	48.37	47.12	0.94	0.89
3H-5, 137–139	22.17	32.34	24.43	1.97	1.93	2.82	2.71	1.49	1.46	47.06	46.07	0.89	0.85
3H-6, 64–66	22.94	36.51	26.75	1.93	1.88	2.86	2.70	1.42	1.38	50.47	49.04	1.02	0.96
3H-6, 136–138	23.66	25.71	20.45	2.11	2.04	2.90	2.73	1.68	1.62	42.14	40.67	0.73	0.69
3H-7, 35–37	24.15	25.33	20.21	2.08	2.03	2.82	2.70	1.66	1.62	41.10	39.98	0.70	0.67
3H-7, 53–55	24.33	25.29	20.19	2.06	2.03	2.76	2.69	1.64	1.62	40.51	39.92	0.68	0.66
4H-1, 52–54	24.82	31.14	23.75	2.00	1.96	2.85	2.75	1.53	1.50	46.44	45.48	0.87	0.83
4H-1, 111–113	25.41	30.80	23.54	2.00	1.98	2.84	2.78	1.53	1.51	46.06	45.51	0.85	0.84
4H-2, 50–52	26.30	36.12	26.53	1.94	1.90	2.86	2.75	1.42	1.40	50.20	49.24	1.01	0.97
4H-2, 73–75	26.53	31.94	24.21	2.00	1.97	2.88	2.78	1.52	1.49	47.32	46.42	0.90	0.87
4H-3, 39–41	27.69	16.58	14.22	2.25	2.21	2.80	2.73	1.93	1.90	31.18	30.66	0.45	0.44
4H-3, 116–118	28.46	15.12	13.14	2.31	2.26	2.84	2.76	2.00	1.96	29.54	28.96	0.42	0.41
4H-4, 67–69	29.47	15.15	13.16	2.28	2.23	2.79	2.72	1.98	1.94	29.21	28.65	0.41	0.40
4H-4, 123–125	30.03	35.32	26.10	1.96	1.91	2.88	2.76	1.45	1.41	49.81	48.75	0.99	0.95
5H-1, 18–20	31.18	23.25	18.87	2.12	2.09	2.81	2.76	1.72	1.70	38.95	38.53	0.64	0.63
5H-1, 146–148	32.46	42.36	29.75	1.89	1.85	2.93	2.82	1.33	1.30	54.78	53.83	1.21	1.17
5H-2, 16–18	32.66	28.84	22.38	1.77	2.02	2.24	2.82	1.37	1.57	38.63	44.21	0.63	0.79

Table 12 (continued).

Core, section, interval (cm)	Depth (mbsf)	WC-d (%)	WC-w (%)	WBD[a] (g/cm^3)	WBD[b] (g/cm^3)	GD[a] (g/cm^3)	GD[b] (g/cm^3)	DBD[a] (g/cm^3)	DBD[b] (g/cm^3)	Por[a] (%)	Por[b] (%)	VR[a]	VR[b]
5H-3, 19–21	34.19	29.90	23.02	1.91	1.96	2.59	2.70	1.47	1.51	43.01	44.05	0.75	0.79
5H-3, 132–134	35.32	25.94	20.60	2.05	2.01	2.76	2.69	1.62	1.60	41.11	40.49	0.70	0.68
5H-4, 71–73	36.21	33.55	25.12	1.97	1.95	2.85	2.78	1.47	1.46	48.23	47.69	0.93	0.91
5H-5, 70–72	37.70	32.15	24.33	2.25	1.94	3.67	2.73	1.71	1.47	53.51	46.16	1.15	0.86
5H-6, 69–71	39.19	31.65	24.04	2.08	1.96	3.09	2.76	1.58	1.49	48.82	46.04	0.95	0.85
5H-7, 12–14	40.12	38.59	27.84	1.60	1.87	2.05	2.73	1.16	1.35	43.57	50.69	0.77	1.03

Notes: WC-d = water content (% dry sample weight); WC-w = water content (% wet sample weight); WBD = wet-bulk density; GD = grain density; DBD = dry-bulk density; Por = porosity; VR = void ratio.

[a]Value calculated using Method B.

[b]Value calculated using Method C.

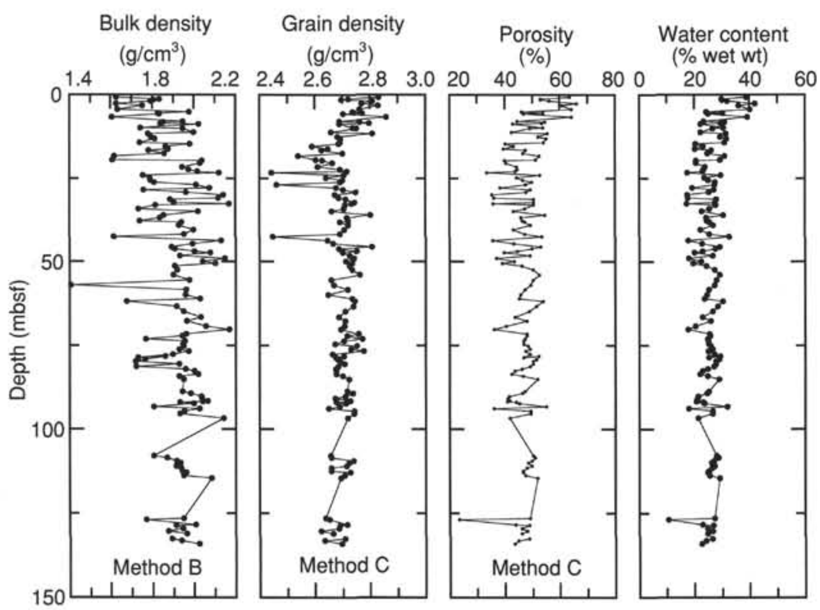

Figure 24. Comparison of laboratory index property measurements vs. depth in Hole 912A.

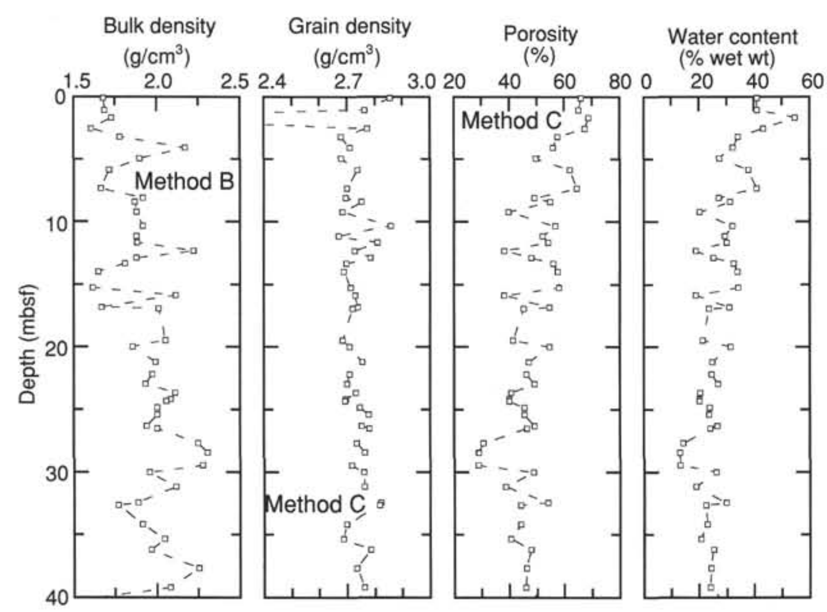

Figure 25. Comparison of laboratory index property measurements vs. depth in Hole 912B.